

Development and Evaluation of 3D Reconstruction Framework for General Objects

by

Kai Wu

Bachelor of Engineering, Beijing University of Posts and Telecommunications

2014

A THESIS SUBMITTED IN PARTIAL FULFILLMENT
OF THE REQUIREMENTS FOR THE DEGREE OF

Master of Applied Science

in

THE FACULTY OF APPLIED SCIENCE
(Electric and Computer Engineering Department)

The University of British Columbia
(Vancouver)

April 2017

© Kai Wu, 2017

Abstract

This document provides brief instructions for using the `ubcdiss` class to write a UBC-conformant dissertation in L^AT_EX. This document is itself written using the `ubcdiss` class and is intended to serve as an example of writing a dissertation in L^AT_EX. This document has embedded Unique Resource Locators (URLS) and is intended to be viewed using a computer-based Portable Document Format (PDF) reader.

Note: Abstracts should generally try to avoid using acronyms.

Note: at University of British Columbia (UBC), both the Graduate and Postdoctoral Studies (GPS) Ph.D. defence programme and the Library's online submission system restricts abstracts to 350 words.

Preface

At UBC, a preface may be required. Be sure to check the GPS guidelines as they may have specific content to be included.

Table of Contents

| | |
|---|-------------|
| Abstract | ii |
| Preface | iii |
| Table of Contents | iv |
| List of Tables | viii |
| List of Figures | x |
| Glossary | xiv |
| Acknowledgments | xv |
| 1 Introduction | 1 |
| 1.1 Outline | 2 |
| 1.1.1 Related Work | 3 |
| 1.1.2 Taxonomy of 3D Reconstruction | 3 |
| 1.1.3 Description of 3D Reconstruction | 4 |
| 1.1.4 Mapping of 3D Reconstruction | 4 |
| 1.1.5 Interpretation of 3D Reconstruction | 4 |
| 1.2 Contributions | 5 |
| 1.3 Organization | 6 |
| 2 Related Work | 8 |
| 2.1 ToolBoxes | 8 |

| | | |
|----------|--|-----------|
| 2.2 | 3D Reconstruction Techniques | 8 |
| 2.2.1 | Stereo Correspondence | 9 |
| 2.2.2 | Shading | 13 |
| 2.2.3 | Silhouette | 17 |
| 2.2.4 | Texture | 19 |
| 2.2.5 | Defocus | 20 |
| 3 | A taxonomy of 3D Reconstruction | 22 |
| 3.1 | New Perspective | 23 |
| 3.2 | Problem Space | 23 |
| 3.3 | Object class | 23 |
| 3.4 | Class 1 | 24 |
| 3.4.1 | SfS | 24 |
| 3.4.2 | Lambertian PS: uniform reflectance | 26 |
| 3.4.3 | SL | 26 |
| 3.5 | Class 2 | 26 |
| 3.5.1 | Non-Lambertian PS: uniform reflectance | 27 |
| 3.6 | Class 3 | 27 |
| 3.6.1 | MVS | 28 |
| 3.6.2 | Lambertian PS: non-uniform reflectance | 28 |
| 3.7 | Class 4 | 29 |
| 3.8 | Class 5 | 30 |
| 3.8.1 | Non-Lambertian PS: non-uniform reflectance | 30 |
| 3.9 | Class 6 | 31 |
| 3.9.1 | VH | 32 |
| 3.10 | Summary | 32 |
| 4 | A Description of 3D Reconstruction | 34 |
| 4.1 | Definition | 35 |
| 4.1.1 | Basic notations | 35 |
| 4.1.2 | Segment and Scell | 35 |
| 4.1.3 | Photo-consistency | 37 |
| 4.1.4 | Formal Definition | 37 |

| | | |
|----------|---|-----------|
| 4.1.5 | Applied Definition | 38 |
| 4.2 | Model | 38 |
| 4.3 | Representation | 39 |
| 4.3.1 | Texture | 39 |
| 4.3.2 | Lightness | 40 |
| 4.3.3 | Reflectance | 43 |
| 4.3.4 | Roughness | 43 |
| 4.3.5 | Concavity | 45 |
| 4.4 | Expression | 45 |
| 5 | A Mapping of 3D Reconstruction | 47 |
| 5.1 | Synthetic setup | 48 |
| 5.2 | Structure of Datasets | 48 |
| 5.3 | Selected methods | 49 |
| 5.4 | Evaluation metrics | 49 |
| 5.5 | Dependency Check | 50 |
| 5.5.1 | PMVS | 50 |
| 5.5.2 | Property and Reconstruction | 50 |
| 5.5.3 | Example-based PS | 54 |
| 5.5.4 | Property and Reconstruction | 54 |
| 5.5.5 | Gray-code SL | 58 |
| 5.5.6 | Property and Reconstruction | 60 |
| 5.6 | Training | 61 |
| 5.6.1 | PMVS | 62 |
| 5.6.2 | Example-based PS (EPS) | 63 |
| 5.6.3 | Gray-code SL (GSL) | 64 |
| 5.7 | Mapping | 66 |
| 6 | An Interpretation of 3D Reconstruction | 68 |
| 6.1 | Evaluation Methodology | 69 |
| 6.1.1 | Objective | 69 |
| 6.1.2 | Key Evaluation Questions and Steps | 69 |
| 6.2 | Parameter Setting | 70 |

| | | |
|-------|--|-----------|
| 6.3 | Effectiveness of Mapping | 70 |
| 6.3.1 | Synthetic Datasets | 70 |
| 6.3.2 | Real-world Datasets | 72 |
| 6.4 | Robustness of Mapping | 74 |
| 6.5 | Summary | 74 |
| | Bibliography | 76 |
| | A Supporting Materials | 82 |
| A.1 | Material of real-world objects | 82 |
| A.2 | Parameters of real-world objects | 82 |
| A.3 | Results of real-world objects | 82 |

List of Tables

| | | |
|-----------|--|----|
| Table 5.3 | Property settings of the pairwise conditions used for the dependency check of the Photometric Stereo algorithms. | 54 |
| Table 5.4 | The correlation between each property and the metric <i>angular difference</i> | 57 |
| Table 5.5 | Property settings of the pairwise conditions used for the dependency check of the Structured Light algorithms. | 60 |
| Table 5.6 | The correlation between each property and the metrics <i>accuracy</i> and <i>completeness</i> | 61 |
| Table 5.7 | The conditions under which PMVS works well in terms of the two metrics <i>accuracy</i> and <i>completeness</i> | 64 |
| Table 5.8 | The conditions under which example-based PS works well in terms of the two metric <i>angular difference</i> | 65 |
| Table 5.9 | The conditions under which Gray code SL works well in terms of the two metrics <i>accuracy</i> and <i>completeness</i> | 65 |
| Table 6.1 | Property lists of the test objects. | 71 |
| Table 6.2 | Property list for the real-world objects | 74 |
| Table A.1 | Material of Real-world objects. | 83 |
| Table A.2 | Property list for the real-world objects | 85 |

List of Figures

| | | |
|------------|---|----|
| Figure 1.1 | Taxonomy of 3D reconstruction algorithms and its dimensions. | 3 |
| Figure 1.2 | Thesis overview. Rectangles denote process. Rounded rectangles represents data or component.[To be re-done] | 7 |
| Figure 2.1 | Illustratives of MI-based VH. (a) shows one object (top left) and its silhouette with 2D lines traced over it to find intersections along rays in the X, Y and Z ray-set of the MI, respectively. (b) shows the MI data structure and conversion algorithm in a 2D example. Image courtesy of M. Tarini. | 18 |
| Figure 2.2 | Three distortion effect: distance distortion, position distortion, and foreshortening distortion. | 19 |
| Figure 2.3 | A thin lens of focal length f focuses the light from a plane a distance z_0 in front of the lens at a distance z_i behind the lens, where $\frac{1}{z_o} + \frac{1}{z_i} = \frac{1}{f}$. If the sensor plane moved forward Δz_i , the image are no longer in focus and the <i>circle of confusion</i> c depends on the distance of the sensor plane motion Δz_i relative to the lens aperture diameter d | 20 |
| Figure 2.4 | shape from focus | 21 |
| Figure 3.1 | <i>Top:</i> A list of properties for object classes. <i>Bottom:</i> Six object classes of interest. Only texture, lightness, and reflectance are consider. Properties not consider are set as follows: opaque, rough (for Lambertian)/smooth (for Non-Lambertian), low concavity. | 25 |

| | | |
|------------|---|----|
| Figure 3.2 | The effect of GBR ambiguity | 29 |
| Figure 4.1 | Relation between a scell and a segment | 36 |
| Figure 4.2 | Light-matter interaction | 41 |
| Figure 4.3 | The light-matter interaction. | 42 |
| Figure 4.4 | The light-lens interaction. | 42 |
| Figure 4.5 | The light-sensor interaction. | 42 |
| Figure 4.6 | A red specular sphere. The surface reflects light in a mirror-like way, and no diffuse reflection exist, thus the colour of the surface is no longer visible. | 44 |
| Figure 4.7 | Surface Slope Distribution Model | 45 |
| Figure 5.1 | Performance of PMVS under six pairwise conditions. For instance, (a) shows the performance under changing <i>texture</i> and <i>albedo</i> values. The property values are assigned based on (a) of Table 5.1. | 51 |
| Figure 5.2 | (a) shows the reflection of light off a specular surface. V_1 received the diffuse component while V_2 receives the specular component. (b), (c) shows the images observed from these two views. The specular area (red circle) observed in V_2 is visible in V_1 | 52 |
| Figure 5.3 | (a)-(c). The albedo is set as 0.2, (d)-(f). the specular is set as 0.2. According to energy conservation, as the specular component increases, the diffuse component decreases. | 53 |
| Figure 5.4 | Performance of Example-based PS under six pairwise conditions. For instance, (a) shows the performance under changing <i>texture</i> and <i>albedo</i> values. The property values are assigned based on Table 5.3 (a). | 55 |
| Figure 5.5 | (a)-(c). The texture is set as 0.5. According to energy conservation, as the specular component increases, the diffuse component decreases. | 56 |

| | | |
|-------------|--|----|
| Figure 5.6 | (a)-(c). The albedo is set as 0.2, (d)-(f). the specular is set as 0.2. According to energy conservation, as the specular component increases, the diffuse component decreases. | 57 |
| Figure 5.7 | The ‘peculiar’ effect of roughness on PS. The order of the property is: albedo, specular, and roughness, thus 080205 means albedo: 0.8, specular: 0.2, and roughness: 0.5 | 58 |
| Figure 5.8 | Performance of Gray-encoded SL under six pairwise conditions. For instance, (a) shows the performance under changing <i>texture</i> and <i>albedo</i> values. The property values are assigned based on Table 5.5 (a). | 59 |
| Figure 5.9 | (a)-(c). The albedo is set as 0.2, (d)-(e). the specular is set as 0.2. According to energy conservation, as the specular component increases, the diffuse component decreases. | 61 |
| Figure 5.10 | (a)-(c). The roughness is set as 0.2, (d)-(e). the specular is set as 0.8. According to energy conservation, as the specular component increases, the diffuse component decreases. | 62 |
| Figure 5.11 | Performance of MVS with varied properties. | 63 |
| Figure 5.12 | Performance of PS with varied properties. | 66 |
| Figure 5.13 | Performance of SL with varied properties. | 67 |
| Figure 6.1 | The UI of determining the albedo, specular, and roughness of the surface. The albedo is set as around 0.8, which is determined by the value channel of HSV colour. The specular and roughness is set as 0.5, 0.2, respectively. (a) demonstrates the effect of the property setting on a sphere while (b) on a teapot. | 71 |
| Figure 6.2 | The synthetic datasets and groundtruth for the evaluation . . . | 72 |
| Figure 6.3 | The first column shows the best algorithm chosen by the mapping. The quantitative and qualitative performance of each technique on the synthetic dataset. The red dots are from the ground truth while the black ones the reconstruction. | 73 |
| Figure 6.4 | The rerepresentatives of the six classes of objects used for evaluation. | 74 |

| | | |
|------------|--|----|
| Figure 6.5 | The evaluation of the effectiveness of the mapping using real-world object. The well reconstructed object is label by red rectangle. | 75 |
| Figure A.1 | Reconstruction results of MVS, PS, SL | 84 |
| Figure A.2 | Reconstruction results of MVS, PS, SL (cont'd) | 85 |

Glossary

This glossary uses the handy `acronym` package to automatically maintain the glossary. It uses the package's `printonlyused` option to include only those acronyms explicitly referenced in the `LATEX` source.

GPS Graduate and Postdoctoral Studies

PDF Portable Document Format

URL Unique Resource Locator, used to describe a means for obtaining some resource on the world wide web

Acknowledgments

Thank those people who helped you.

Don't forget your parents or loved ones.

You may wish to acknowledge your funding sources.

Chapter 1

Introduction

Modelling of the 3D world has been an active research topic in computer vision for decades. The goal is to reconstruct a 3D geometric model, represented by point cloud, voxel grid, depth maps, or surface mesh, from RGB or range sensors, optionally with the material of the surface. It has a wide range of applications including 3D mapping and navigation, online shopping, 3D printing, computational photography, video games, visual effects, and cultural heritage archival.

This is an extremely challenging task since it's the reverse process of image formation, which is highly likely to have more than one plausible results. To overcome this challenge, some assumptions have to be made in terms of the materials, viewpoints, and lighting. Thus A solid understanding of the interaction of lighting with surface geometry and material is a prerequisite to fully take advantage of the existing techniques. In the past decades, we've witness a variety of tools and approaches such as Computer Aided Design (CAD) tools [1], arm-mounted probes, active methods [2, 3, 12, 33] and passive image-based methods [18, 20, 23, 32] applied successfully to some sub-domains of the problem. Among the existing techniques, active techniques such as laser scanner [33], structured light system (SL) [12], and Photometric Stereo (PS) [61], and passive method such as Multi-view Stereo (MVS) [50] have been the most successful ones. Laser scanners and structured light techniques can generate the most accurate results, but is generally complicated to set up and calibrate, time consuming to scan, and memory demanding to store and process. Photometric Stereo is able to achieve highly detailed

reconstruction comparable to that of laser scanner, but the true depth information is lost due to the use of a single viewpoint. MVS requires minimal setup and can work in both controlled, small scale lab settings or outdoor, medium to large scale environments. However, the quality of the reconstruction is generally noisier, and is susceptible to the texture and material property of the surface. All these techniques require an understanding of calibration, stereo correspondence, physics-based vision, and etc, which is no easy task to master.

Regardless of the past success and the strong demands in various areas, we have not yet witnessed any substantial progress in terms of making those techniques accessible to application developers who generally have little or no computer vision expertise. We've made two key observations about computer vision algorithms: 1) none of these methods works well under all circumstances, nor do they require the same setup or inputs/outputs, making it difficult for developers to choose the optimal method for their particular application; 2) expertise knowledge is a prerequisite to fully exploit the potentials of existing vision techniques. These observations lead us to the question: is it possible to create a framework that can select the best possible algorithm based on the descriptions of the object or scene to be reconstructed. The mental model to our approach is similar to that of the game ‘name that object’: one participant takes guesses of what the object is based solely on the descriptions of the appearance provided by the other participant. In our case, the key idea is to construct an algorithm-free framework above the algorithms so that one or multiple best suited ones can be selected based on the ‘appearance’ of the object described by the developers. The developers use the framework’s description interface that is structured to match how vision problems can be described based on a model of a 3D scene and translated to parameters useful for determining which algorithms would work best.

1.1 Outline

The problem that this thesis addresses can be described as: construct a framework for 3D reconstruction that maps the description of the problem condition to the best possible algorithm from a suite of algorithms. First the development of the framework is discussed, which ultimately maps from a well defined problem space

to a suite of algorithms, and then a rigorous evaluation is carried out to verify the effectiveness and robustness of the derived mapping. More specifically, a new taxonomy transforms the 3D reconstruction problem from one requiring knowledge of algorithmic details to one that is based on the mapping between the problem space and algorithms. Then a well defined model and representations are developed to describe the problem space definitively. Lastly, the mapping bewteen the problem space and algorithms are discovered, from which a mapping is derived. More detailed descriptions and flow charts are presented below to provide an overview of the framework and the thesis.

1.1.1 Related Work

We discuss the existing softwares and toolboxes for 3D reconstruction, and present the required vision background needed to fully take advantage of those toolboxes. A review of the 3D acquisition techniques is provided, organized by the visual and geometric cues used for reconstruction.

1.1.2 Taxonomy of 3D Reconstruction

The proposed taxonomy categorizes algorithms based on how well they work on the specific problem condition. First the problem space is developed, with each axis represents a key property of object's material or geometry. Then the selected classes of algorithms are mapped to selected problem conditions based on reports in the literature.

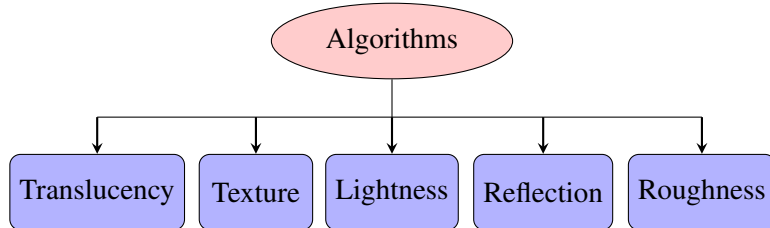


Figure 1.1: Taxonomy of 3D reconstruction algorithms and its dimensions.

1.1.3 Description of 3D Reconstruction

We provide a rigorous definition of the problem space. First, a formal and practical definition of the 3D reconstruction problem based on set theory is proposed. Second, a model consists of key properties of an object is developed. Third, the representations of the problem are proposed: we select key elements that can affect the properties of the model and use them as the components of the representation. Lastly, common 3D reconstruction tasks are expressed using the proposed model and representations.

1.1.4 Mapping of 3D Reconstruction

Since the problem space was not well defined, the mapping from problem space to algorithms is ambiguous. To derive more accurate mapping, we need to evaluate the performance of the selected algorithms under varied properties and their combinations. We use synthetic datasets to achieve this goal. Part of the challenge in establishing a comprehensive set of experiments for such an evaluation is the large variability of shapes and material properties. To overcome this issue, we first investigate the dependent properties, which are properties that have influence on one another, thus must be considered jointly. Then we evaluate the performance of each algorithm under the conditions of dependent properties and all their combinations, which makes up our abstraction.

1.1.5 Interpretation of 3D Reconstruction

To test the effectiveness and robustness of the derived mapping, three key questions need to be answered: 1). can the mapping return the best possible result given the description; 2). how useful is the derived mapping compared to the traditional approaches; 3). what limitations does the current mapping have. To answer these questions, we carry out separate steps: 1). we use both synthetic and real-world datasets to see if the quantitative and qualitative results is consistent with the algorithm returned by the mapping; 2). we simulate a practical scenario of applying 3D reconstruction and see how accessible each step is individually; 3).

1.2 Contributions

The main contribution of the thesis is the development and evaluation of a framework that maps the description of the problem condition to the best possible algorithm from a suite of algorithms. It is non-trivial for two reasons: 1). currently, no one approach can achieve satisfactory result for an object with general material and geometric properties, the derived mapping can, to some extend, solve this problem by incorporating multiple algorithms into the framework; 2). a solid understanding of the algorithmic details of reconstruction algorithms is a prerequisite to fully take advantage of the existing techniques, which is unattainable for general developers, the descriptive language proposed in the thesis can allow application developer bypass this hurdle thus is more developer-friendly. The significant aspects are presented below:

1. A new taxonomy of 3D reconstruction problem that focuses on problem conditions instead of algorithmic details.

Most taxonomies generally focus on one class of algorithms, and classify intra-class algorithms based on differences of the algorithmic details. For instance, MVS algorithms can be categorized based on visibility models or scene representations, and PS methods can be classified by the reflectance models. However, it doesn't provide the context or the conditions where these techniques perform well, which is crucial when it comes to design an application that requires reliable reconstruction techniques.

2. A formal definition of the problem space and description of 3D reconstruction that allows more accurate mapping.

The research of the vision has always been focused on technical novelties. However, we started to lose sight of the big picture and . Therefore, it's crucial to have a better understanding of the problem space to exploit the strengths and weaknesses of existing techniques. Besides, it shows the researchers the lack of progress in certain areas thus is helpful to redirect research efforts to less explored territories.

Knowledge of which algorithm performs best from amongst those that target the conditions of a particular application area is similarly empirical and is often contentious as the conditions or images used to represent those conditions are often

not the same. Binary classification of a problem type does not allow for the level of distinction required to know how effective a given algorithm will be within a particular range of the problem space. This information also changes regularly as new algorithms are developed. Without a model of the image registration problem space, expressing the conditions of a given problem is not a well defined process.

3. The development and evaluation of the mapping of 3D reconstruction.

The construction of the mapping allows more accurate mapping. However, different from the previous research working on algorithms, the evaluation is more complicated and sophisticated. The reason for such an evaluation is that the mapping is for more general objects and algorithms, thus it requires a wider test cases, and rigorous experiment design.

1.3 Organization

We organize this thesis as follows: we discuss the related work in Chapter 2. In Chapter 3 we provide a new taxonomy of 3D reconstruction based on the mapping from problem space to algorithms. In Chapter 4, we provide a formal description of the 3D reconstruction problem, which can be applied to the currently existing techniques, and extended to future algorithms. In Chapter 5, we discuss the process of generating a synthetic dataset to evaluate the performance of a selected set of techniques under varied problem conditions, from which a mapping is derived for 3D reconstruction. In Chapter 6, we use both synthetic and real-world datasets to demonstrate the interpretation of the 3D reconstruction description and the validity of the proposed mapping.

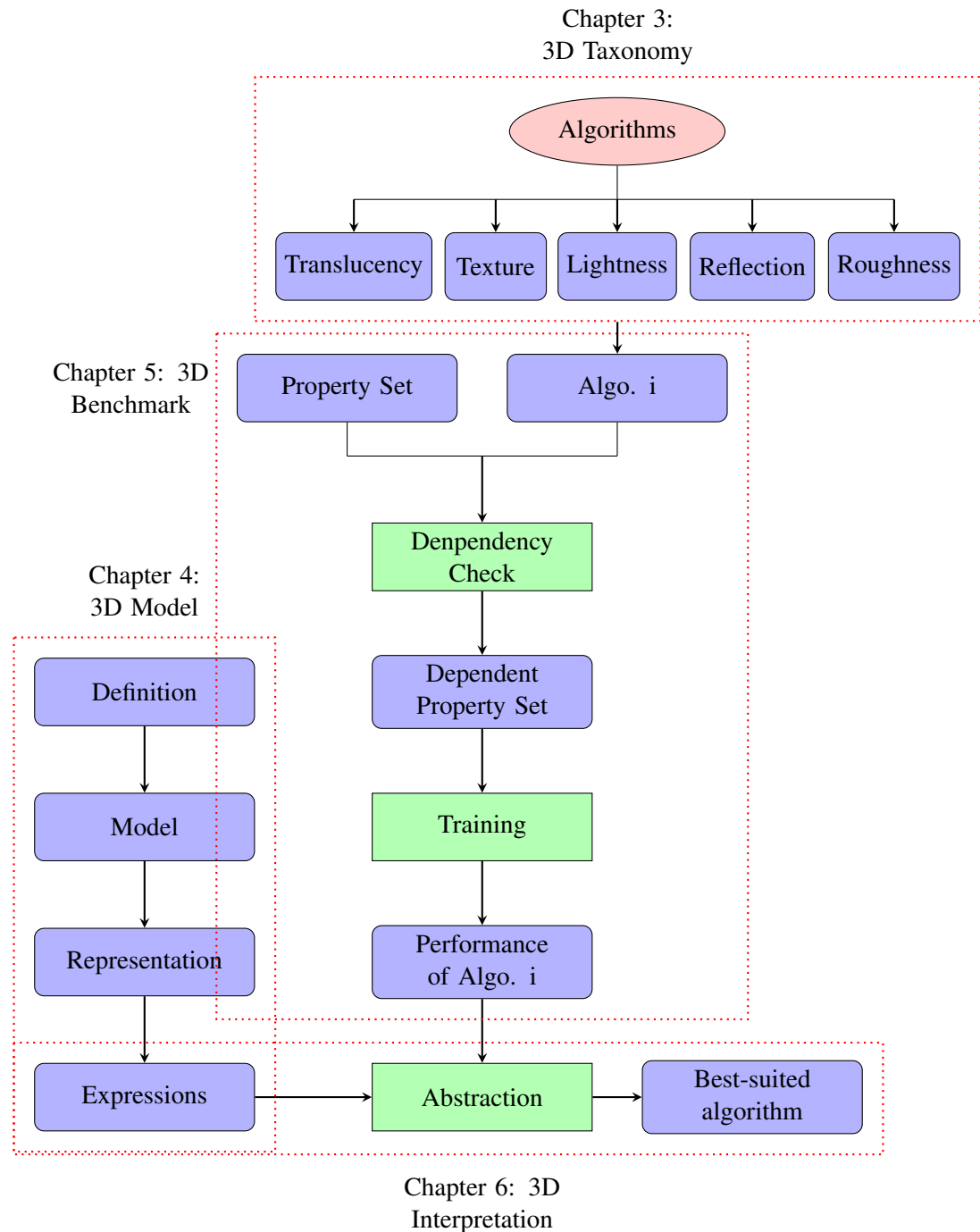


Figure 1.2: Thesis overview. Rectangles denote process. Rounded rectangles represent data or component.[To be re-done]

Chapter 2

Related Work

Section 2.1 discusses the existing toolboxes for 3D reconstruction. Section 2.2 presents a comprehensive review of the field of image-based 3D reconstruction based on varied visual/geometric cues, which include *stereo correspondence, shading, silhouette, texture distortion, and (de)focus*.

2.1 ToolBoxes

There have been many attempts in developing computer vision or image processing frameworks that support rapid development of vision applications. There are multiple general vision libraries in the field including OpenCV [15], VLFeat [57], VXL [4] and multiple Matlab libraries [31, 38]. These libraries often provide tools to multiple image processing and computer vision problems, including low-vision tasks such as feature detection and matching, middle-level vision tasks such as segmentation, tracking, and high-level vision problems such as classification and recognition. All of these software frameworks and libraries provide vision components and algorithms without any context of how and when they should be applied, and so often require expert vision knowledge for effective use.

2.2 3D Reconstruction Techniques

Image-based 3D reconstruction attempts to recover the geometry and optionally the material of the object from images under different viewpoints or illuminations.

The goal can be described as “given a set of images of an object or a scene, estimate the most likely 3D shape that explains those images, under the assumption of known materials, viewpoints, and lighting conditions”. This definition reveals that if those assumptions are violated, this becomes an ill-posed problem since multiple combinations of geometry, viewpoint and illumination can produce exactly the same images [43], thus making it an extremely challenging task.

The 3D reconstruction techniques exploits a variety of visual and geometric cues to extract geomtry from images: stereo correspondence, shading, contour, texture, (de)focus, etc, please refer to Table 2.1 for an overview. The algorithms are organized based on the cue used for reconstruction.

| Cue | Algorithm |
|-----------------------|--|
| Stereo correspondence | Stereoscopy Trinocular Stereo Multi-view Stereo (MVS) Laser scanning Structured light (SL) |
| Shading | Shape from Shading (SfS) Photometric Stereo (PS) |
| Contour | Shape from Silhouette (SfS) |
| Texture | Shape from Texture |
| (De)focus | Shape from (De)focus |

Table 2.1: Classes of algorithms that utilize each visual/geometric cue. Note that the abbreviations will be used extensively in the theis, and the actuall meaning of SfS can be deduced from the context.

2.2.1 Stereo Correspondence

Stereo correspondence is one of the most widely used visual cues in 3D vision. Passive methods, including stereoscopy, trinocular stereo, and MVS, identify correspondences across different views, and estimate the 3D point by triangulation. However these passive approaches suffer from uniform or periodic surfaces. The active techniques attempt to overcome the correspondence problem by replacing one of the cameras with a controllable illumination source, e.g., single-point laser, slit laser scanner, and temporal or spatially modulated Structured Light (SL), we

refer the readers to the survey article by Blais for recent development of active methods. Two most popular methods, MVS and SL, are reviewed in depth, and organized based on the reconstruction algorithms and projection patterns used, respectively.

Volumetric methods

The first class computes the cost function in a 3D volume, then extracts a surface from this volume. One successful algorithm is voxel colouring, which traverses a discretized 3D space in depth-order to identify voxels that have a unique colouring, constant across all possible interpretations of the scene [49]. Another thread of work formulates the problem in the Markov Random Field (MRF) framework and extracts the optimal surface by Graph-Cut algorithms [45, 58, 59].

Surface Evolution

The second class works by iteratively evolving a volume or surface to minimize a cost function. The class includes methods based on voxels, level set, and surface meshes. Space Carving technique achieves least-commitment shape [39] by iteratively removing inconsistent voxels from the scene [32]. Level-set techniques cast the problem as a variational one, and use a set of PDE's as cost functions, which are deformed from an initial set of surfaces towards the objects to be detected [18]. Other approaches use a deformable model and represent the scene as surface meshes that moves as a function of internal and external forces [17]. Hiep et al. presented a visibility-based method that transforms a dense point cloud into a surface mesh, which is feed into a mesh-based variational refinement that captures small details, smartly handling photo-consistency, regularization and adaptive resolution.

Region Growing

The third class starts with a sparse set of scene points, and propagates these points to spatial neighbours and refine the cost function with respect to position and orientation of the points. Otto and Chau proposed one of the first work on region growing stereo search. The essence of the algorithm is: start with an approximate match

between a point in one image and a point in another, use an adaptive least-squares correlation algorithm to produce a more accurate match, and use this to predict approximate matches for points in the neighbourhood of the first match. A two-view quasi-dense approach first sorts the list of point correspondences into a list of seed points by correlation score. At each step of the propagation, A ‘best’ seed point is chosen. Then in the immediate spatial neighborhood of this seed point, new potential matches are checked and the bests are added to the current list of seed points [34, 35]. This best-first strategy guarantees convergence by choosing only new matches that have not yet been selected. A patch based approach undergoes multiple iterations of matching, propagation, and filtering [20]. A stereoscopic approach called PatchMatch Stereo, which is inspired by an approximate nearest neighbour matching algorithm called PatchMatch [8]. The method starts by randomly assigning an oriented plane to each pixel in two views. Then each pixel goes through three iterations of propagations and refinement. The plane is propagated to spatial neighbours, corresponding pixel from another view, and across time. It can achieve sub-pixel accuracy, but is computational heavy and difficult to parallelism. There has been some efforts to extend PatchMatch Stereo to multi-view scenario [21, 56, 62] or proposing new propagation scheme to increase the computational efficiency [21].

Depthmap Merging

The fourth class is image-space based methods that computes a per-view depthmap. By treating a depthmap as a 2D array of 3D points, multiple depthmaps can be considered as a merged 3D point cloud. The winner-takes-all approach takes a set of discretised depth values and pick the one with the highest photo-consistency score for each pixel independently. Uniform depth sampling may suffice for simple and compact objects. However, for complex and large scenes, a proper sampling scheme is crucial to achieve high speed and quality. More sophisticated cost function are derived to account for occlusion or non-Lambertian effects which might add noise to the photo-consistency score [23, 59]. In the case of severe occlusion, spatial consistency can be enforced under the assumption that neighbouring pixels have similar depth values. This can be formulated under the Markov Random Field

(MRF) framework, where the problem becomes minimizing the sum of a unary $\Phi(\cdot)$ and pairwise term $\Psi(\cdot, \cdot)$. The unary term reflects the photo-consistency score of assigning a depth value d_p from a depth set to the pixel p , whereas the pairwise term enforces the spatial regularization, and assigns the cost of setting depth label k_p, k_q to a pair of neighbouring pixels p and q , respectively.

$$E(\{k_p\}) = \sum_p \Phi(k_p) + \sum_{(p,q) \in \mathcal{N}} \Psi(k_p, k_q)$$

Structured Light

Structured light is considered one of the most accurate reconstruction technique. It is based on projecting a temporally or spatially modulated pattern onto the surface and viewing the illuminated surface from one or more points of view. The correspondence is easily detected from the projected and imaged pattern, which is triangulated to obtain the 3D point. Each pixel in the pattern is assigned a unique codeword, and the codeword is encoded by using grey level, colour or geometric representations. Structured light is classified based on the coding strategy: temporal, spatial and direct codification [46]. Temporal techniques generate the codeword by projecting a sequence of patterns. Spatial codification represents each codeword in a unique pattern. Direct codification techniques define a codeword for every pixel, which is equal to its grey level or colour.

Temporal encoding A sequence of patterns are successively projected onto the surface, the codeword for a given pixel is formed by the sequence of illuminaiton values for that pixel across the projected patterns. This kind of pattern can achieve high accuracy due to two factors: 1). the codeword basis is small, e.g., two for binary pattern, therefore, each bit is easily distinguishable; 2). a coarse-to-fine strategy is used, and the position of the pixel becomes more precise as the patterns are successively projected. We further classify these techniques as follows: 1). binary codeword; 2). n -ary codeword; 3). gray code combined with phase shifting; 4). hybrid techniques.

Spatial encoding This kind of technique concentrate all the coding in a unique pattern. The codeword that labels a certain pixel is obtained from a neighbourhood

of the pixels around it. Normally, the visual features gathered in a neighbourhood are the intensity or colour of the pixels or groups of pixels around it.

Direct encoding There are ways that can directly represent the codeword in each pixel. To achieve this, there is a need to use either a large range of colour values or introduce periodicity. However, this kind of pattern is highly sensitive to noise because the “distance” between codewords is nearly zero. Moreover, the perceived colour depends not only on the projected colour, but also the intrinsic colour of the surface, therefore, reference images must be taken. This kind of coding can be classified as: 1). codification based on grey levels; 2). codification based on colour.

2.2.2 Shading

The shading variations can reveal the surface normal orientation, which can be further integrated into a 2.5D height map. Shading variation depends on the shape (surface normal orientation), reflectance (material), and lighting (illumination), therefore is generally a ill-posed problem because difference shapes illuminated under different light conditions might produce the same image. This leads to a novel technique called Photometric Stereo in which surface orientation is determined from two or more images. The idea of Photometric Stereo is to vary the direction of the incident illumination between successive views while holding the viewing direction constant. This provides enough information to determine surface orientation at each pixel [60]. This technique can produce a surface normal map with the same resolution of the input image, i.e., to produce the pixel-wise surface normal map. Since the coefficients of the normal are continuous, the integrated height map can reach an accuracy that cannot be achieved by any triangulation methods. Therefore, photometric stereo is more desirable if the intrinsic geometric details are of great importance.

Shape from Shading

The problem of recovering the shape of a surface from the intensity variation is first proposed by Horn [28]. It assumes that the surface under consideration is of a uniform albedo and reflectance, and that the direction of the single distant light

source is either known or can be calibrated by the use of a reference object. Thus the intensity $I(x, y)$ becomes purely a function of the local surface orientation. The information of reflectance, illumination, and viewing geometry can be combined into a single function called reflectance map $R(p, q)$, that relates surface orientation directly to image intensities

$$I(x, y) = R(p(x, y), q(x, y))$$

$$I(x, y) = \rho(\vec{n}, \vec{l}) \vec{n}^\top \vec{l} \quad (\text{Lambertian model})$$

where $(p, q) = (z_x, z_y)$ are surface gradients. Unfortunately, measurements of the brightness at a single pixel only provide one constraint whereas surface orientation requires two. Thus additional constraints such as smoothness or integrability is required to estimate (p, q) .

Photometric Stereo

| Category | Camera | Light source | Reflectance |
|----------------------------|--------------|--|----------------|
| Original PS | Orthographic | Directional, known intensity and direction | Lambertian |
| Generalized lighting PS | Orthographic | unknown intensity and direction, ambient | Lambertian |
| Generalized reflectance PS | Orthographic | Distant, known intensity and direction | Non-Lambertian |

Table 2.2: Assumptions made by different classes of photometric stereo.

Original Photometric Stereo This method, first proposed by Woodham [61], utilised multiple light sources from different directions to overcome the ambiguity of Shape from Shading. Assume there are P pixels per image, and Q illumination directions, the intensity of the i th pixel under j th illumination would be

$$I_{i,j} = \rho_i \vec{n}_i^\top \vec{l}_j$$

$$\Rightarrow \mathbf{I} = \mathbf{N}^\top \mathbf{L}$$

where

- $\mathbf{I} \in \mathbb{R}^{P \times Q}$ stores the pixel intensity from all images. Each column contains pixels from each image while each rows contains intensity of each pixel under all illumination conditions

- $\mathbf{N} \in \mathbb{R}^{P \times 3}$ encodes the albedo-scaled surface normal for each pixel, i.e., $N_{i,:} = \rho_i \vec{n}_i^\top$
- $\mathbf{L} \in \mathbb{R}^{3 \times Q}$ encodes the light source directions, i.e., $L_{:,j} = \vec{l}_j$

This surface reflectance, i.e., spatially varying albedo, and the normal can be estimated by

$$\begin{aligned} N &= IL^+ \\ \rho_i &= \|N_{i,:}\| \\ n_i &= \frac{N_{i,:}^\top}{\|N_{i,:}\|} \end{aligned}$$

The key problem is how to generalize the assumptions of photometric stereo. For the camera assumption, orthographic projection can be achieved by using a lens with long focus and placing the objects far from the camera. The nonlinear response can be solved by performing radiometric calibration. The shadow and other global light transportation are one of the sources of errors, some approaches consider them as outliers and remove them before normal estimation. The reflectance and lighting assumptions, however, are the most complicated ones since the reflectance properties depends on material property and the microscopic structure, and the lighting can have arbitrary or fixed position, orientation, and intensity. Therefore the research on Photometric Stereo are generally on two directions: 1). generalization of reflectance; 2). generalization of lighting conditions.

Generalization of Lighting It is possible to estimate the surface orientation without knowing the light directions, a case also known as *uncalibrated Photometric Stereo*, see Table 2.2. Most such techniques assume Lambertian techniques and are based on factorization technique proposed in [25]. Recall the Irradiance equation:

$$I = N^\top L$$

However, an infinite number of candidates \hat{N} and \hat{L} make the above equality met. In fact, any invertible 3×3 matrix G defines a candidate pair $\hat{N} = N \cdot G, \hat{L} = G^{-1}L$. Thus the normal N and light source direction L can only be recovered up to a linear transformation.

Other generalized lighting conditions are anything other than the ideal case of using a single distant point light source in a dark room. Therefore, any general cases like natural ambient light, multiple point light sources with/without ambient lighting, etc. To make the problem more tractable, the reflectance model should no longer be a general one, otherwise, the problem would have too many degrees of freedom, which means many different shapes with an incorrectly estimated general reflectance, and an incorrectly estimated general lighting would generate the same image appearance with much higher probability.

Generalization of Reflectance This class of techniques relax the assumption of Lambertian reflectance.

Outlier rejection The fact that the reflectance of non-Lambertian surfaces can be approximated by the sum of a diffuse and a specular lobe has been exploited extensively. The specular pixels are considered as outliers in [16] and [9]. The assumption that the color of the specular lobe differs from that of the diffuse lobe allows the separation of the specular and diffuse components [37, 47, 48].

Reference object A different approach uses a reference object that has the same material as the target object. This is proposed in [52] and later revisited in [26]. It can deal with arbitrary BRDFs as long as the reference and target object has the same material. Multiple reference objects are needed for spatially-varying BRDFs as the BRDF at each point on the target object is a linear combination of the basis BRDFs defined by the set of reference objects.

Parametric reflectance model More sophisticated BRDF models can replace the reference objects. An isotropic Ward model is used as basis BRDF, and the surface orientation and parameters of the reflectance models are estimated iteratively [24].

Invariants of BRDF While parametric reflectance models are very good at reducing the complexity of BRDFs, they are usually only valid for a limited class of materials. An alternative is to exploit the invariants of BRDFs. Typical ones include energy conservation, non-negativity, Helmholtz reciprocity, isotropy, etc [6, 63].

2.2.3 Silhouette

In some cases, it's an easy task to perform a foreground segmentation of the object of interest, which leads to a class of techniques that reconstructs a 3D volumetric model from the intersection of the binary silhouettes projected into 3D. The resulting model is called a *visual hull*.

The basic idea of shape from silhouette algorithms is that the object lies inside the intersection of all visual cones back-projected from silhouettes. Suppose there are multiple views V of the target object. From each viewpoint $v \in V$, the silhouette s_v can be extracted, which is the region including the object's interior pixels and delimited by the line(s) separating the object from the background. The silhouette s_v are generally non-convex and can represent holes due to the geometry of the object. A cone-like volume $cone_v$ called (truncated) extended silhouette is generated by all the rays starting at the center of projection and passing through all the points of the silhouette. The target object is definitely internal to $cone_v$ and this is true fro every view $v' \in V$; it follows that the object is contained inside the volume $c_V = \cap_{v \in V} c_v$. As the size of the V goes to infinity, and all possible views are included, c_V converges to a shape known as the *visual hull* vh of the target object.

[computational complexity] intersection of many volumes can be slow. Simple polyhedron-polyhedron intersection algorithms are inefficient. To improve performance, most methods 1) quantize volumes, 2) perform intersection computation in 2D instead of 3D.

Voxel based methods

First the object space is split up into a 3D grid of voxels; each voxel is intersected with each silhouette volume; only voxels that lie inside all silhouette volumes remain part of the final shape.

Marching intersections based methods

The marching intersection (MI) structure consists of 3 orthogonal sets of rays, parallel to the X , Y , and Z axis, which are arranged in 2D regular arrays, called the $X-rayset$, $Y-rayset$, $Z-rayset$ respectively. Each ray in each rayset is projected to the image plane to find the intersections with the silhouette. These intersections

are un-projected to compute the 3D intersection between the ray and the extended silhouette on this ray. This process is repeated for each silhouette, and the un-projected intersections on the same ray are merged by the boolean AND operation.

Once the MI data structure representing the intersection of all extended silhouettes, a triangular mesh is extracted from it. This is done by the MI technique proposed in [44] which traverses the “virtual cells” implicitly defined by the MI, builds a proper marching cube (MC) entry for them that in turn is used to index a MC’s lookup table.

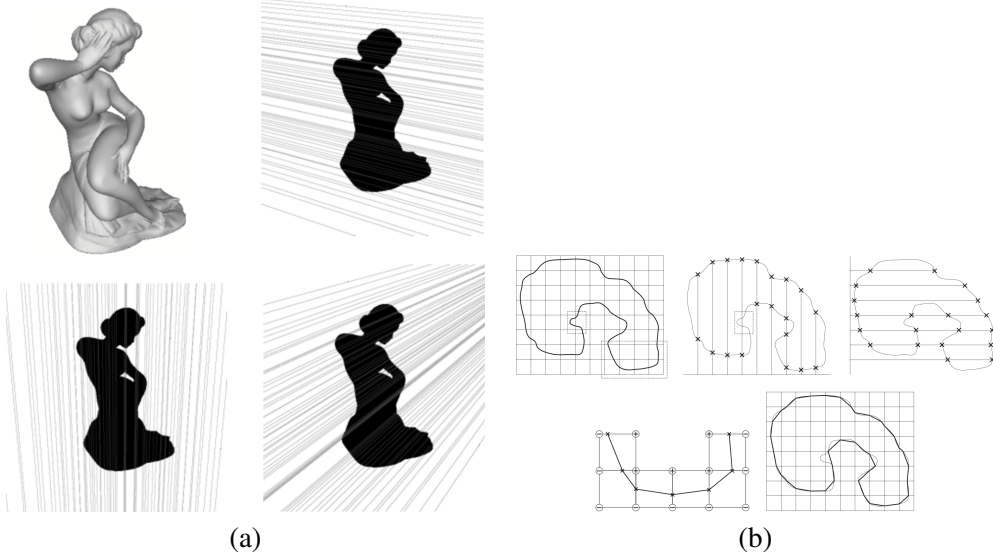


Figure 2.1: Illustratives of MI-based VH. (a) shows one object (top left) and its silhouette with 2D lines traced over it to find intersections along rays in the X, Y and Z ray-set of the MI, respectively. (b) shows the MI data structure and conversion algorithm in a 2D example. Image courtesy of M. Tarini.

Exact polyhedral methods

The silhouette is converted into a set of convex or non-convex 2D polygons with holes allowed. The resulting visual hull with respect to those polygonal silhouettes is a polyhedron. The faces of this polyhedron lie on the faces of the original cones. The faces of the original cones are defined by the center of projections and the

edges in the input silhouettes. The idea of this method is: for each input silhouette s_i we compute the face of the cone. Then we intersect this face with cones of all other input silhouettes, i.e., a polygon-polyhedron intersection. The result of these intersections is a set of polygons that define the surface of the visual hull.

All of the cues above are most widely used ones, and achieved decent results. These following two cues haven't resulted in as much success. Therefore, we only discuss the general idea rather than the technical details.

2.2.4 Texture

The basic principle behind shape from texture is the *distortion* of the individual texel. In general, the image formation process introduces three distortion effects: the *distance effect*, which makes objects in view appear larger when they are closer to the image plane; the *position effect* which makes objects appear differently when the angle between the line of sight and the image plane different; and the *foreshortening effect*, which distort the objects depending on the angle between the surface normal and the line of sight. Besides, different effects take place under different projection models: the orthographic projection captures only the foreshortening effect whereas the perspective projection captures all three. Therefore, shape from texture methods which use orthographic projection are valid only in a limited domain, where the other two effects can be ignored, and the perspective model captures all three effects, but the resulting algorithms are complicated and involves the solution of nonlinear equations.

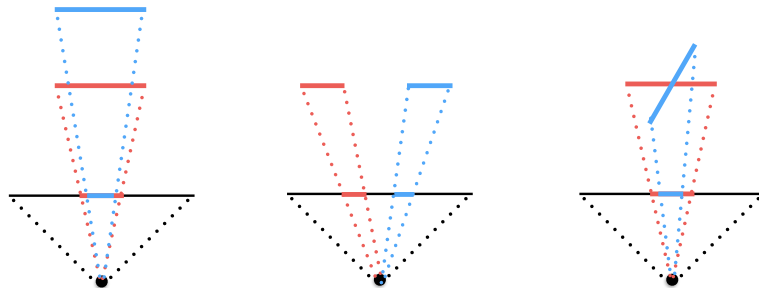


Figure 2.2: Three distortion effect: distance distortion, position distortion, and foreshortening distortion.

To calculate the surface curvature at any point is far from trivial. Therefore, the surface shape is reconstructed by calculating the surface orientation (surface normal). A map of surface normals specifies the surface's orientation only at the points where the normals are computed. But, assuming that the normals are dense enough and the surface is smooth, the map can be used to reconstruct the surface shape.

2.2.5 Defocus

Shape from focus A strong cue for object depth is the amount of blur, which increases as the object moves away from the camera's focusing distance. As shown in Figure 2.3, moving the object surface away from the focus plane increases the circle of confusion.

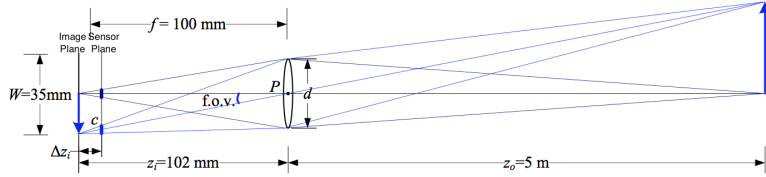


Figure 2.3: A thin lens of focal length f focuses the light from a plane a distance z_o in front of the lens at a distance z_i behind the lens, where $\frac{1}{z_o} + \frac{1}{z_i} = \frac{1}{f}$. If the sensor plane moved forward Δz_i , the image are no longer in focus and the *circle of confusion* c depends on the distance of the sensor plane motion Δz_i relative to the lens aperture diameter d .

Figure 2.3 shows the basic geometric image formation. The relationship between the object distance z_o , focal distance of the lens f , and the image distance z_i , is given by the Gaussian lens law:

$$\frac{1}{z_o} + \frac{1}{z_i} = \frac{1}{f}$$

All light rays that are radiated from the object and intercepted by the lens to converge at a single point on the image plane, thus a *focused* image $I_f(x, y)$ is formed on the image plane. If, however, the sensor plane does not coincide with the image plane and is displaced from the image plane by a distance Δz_i , the energy received from the object is uniformly distributed over a circular patch on the sensor plane.

The relationship between the radius c of the circle of confusion and the sensor displacement Δz_i is as follows:

$$c = \frac{\Delta z_i r}{z_i}$$

The defocused images can be obtained in three ways: by displacing the sensor with respect to the image plane, by moving the lens, or by moving the object with respect to the object plane. The first two ways can cause the following problems:

- The magnification of the system varies, thereby causing the image coordinates of the object points to change.
- The area on the sensor plane over which light energy is distributed varies, thereby causing a variation in image brightness.

To address this issue, the degree of focus is changed by moving the object with respect to a fixed configuration of the optical system and sensor. This approach ensures that the focused areas of the image are always subjected to the same magnification.

The idea is as follows: the stage is moved in increments of Δd , and an image is captured at each stage position ($d = n\Delta d$). By studying the behaviour of the focus measure, an interpolation method is used to compute the accurate depth estimates from a small number of focus measures. An important feature of this method is the local nature, the depth estimate at an image point is computed only from focus measures recorded at that point.

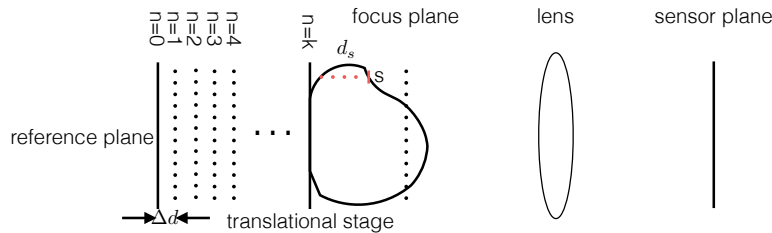


Figure 2.4: shape from focus

Chapter 3

A taxonomy of 3D Reconstruction

Existing taxonomies of 3D reconstruction techniques generally focus on one category of techniques: the Multi-view Stereo taxonomy in [50] proposed classification of MVS algorithms from various perspectives. Reviews of Structured Light techniques generally classify techniques based on the type of projection pattern used [22, 46]. Photometric Stereo algorithms are classified by the assumptions or generalizations made, for instance, unknown/known reflectance, unknown/known light conditions (uncalibrated/calibrated), etc [51]. These frameworks provide a way to categorize intra-category algorithms, but is unsuitable to evaluate the performance of inter-category algorithms. Furthermore, the algorithms under consideration are targeted at a limited categories of objects. It's well known that these algorithms are highly likely to fail on other categories of objects, and this knowledge of algorithmic applicability is largely empirical, with each algorithm roughly maps to a problem domain that is poorly defined. Thus we need a more object-centered approach to the taxonomy so that a more precise mapping is available.

It's crucial to understand where algorithms perform well and where they fail when designing an application for reconstruction. Under the previous framework of taxonomy, this knowledge is largely empirical, with each algorithm mapped roughly to a sub-volume in the problem space. However, this mapping is ambiguous, i.e., the sub-space is not well defined, and also too general, i.e., algorithm within the same category cannot be effectively distinguished. To overcome this limitation, we need to 1). propose a well-defined problem space; 2). bypass

the algorithmic details and focus on properties that are not intuitive to understand and perceive.

The taxonomy proposed in this chapter defines the 3D reconstruction techniques from a object-centered viewpoint, i.e., categorize algorithm based on object class. This taxonomy transforms the 3D reconstruction problem from one requiring knowledge and expertise of specific algorithms in terms of how and when to use them, to one requiring knowledge of the visual and geometric properties of the target object. We first propose a n -dimensional problem space where each dimension is

3.1 New Perspective

Most previous taxonomies categorize algorithms based on the algorithmic details. However, this approach 1). gives very little insight as what conditions does a specific algorithm work well; 2). requires vision knowledge to understand and use these algorithms.

The new perspective approaches the taxonomy from a different angle.

3.2 Problem Space

The dimension of the problem space should be orthogonal, and

3.3 Object class

In Figure 3.1 (a), we show a taxonomy of object classes with different material and shape properties. There are in total $3 \times 3 \times 2 \times 4 \times 2 \times 5 = 720$ classes of objects, which still don't fully capture the variations exhibited by real world objects, for instance, effects such as occlusion, discontinuity, emission, etc are not considered. Most techniques that have been developed over the past decades can only tackle a subset of all possible object classes, with a focus on opaque, diffuse objects. For specular, refractive, and translucent or transparent objects, only very specialized algorithms are applicable for reconstruction [29].

To make the problem tackleable, only six classes of objects are being investigated in depth. The reasoning behind the selected object classes is solely based on

the [popularity] of the class. See Figure 3.1 (b) for the six classes of objects.

Here is a list of algorithms we will look into in depth, a summary is list in Table 3.1.

| Algo. class | Technique |
|--------------------|--|
| SfS | Horn [28] |
| MVS | Furukawa [20], Goesele [23], Vogiatzis [59], Hernández [17], Faugeras [18] |
| Lamberian PS | Woodham [61], Hayakawa [25], Belhumeur [10], Alldrin [7] |
| Non Lambertian PS | Coleman [16], Barsky [9], Schluns [48], Sato [47], Mallick [37], Alldrain [5], Goldman [24], Silver [52], Hertzmann [26], Zickler [63] |
| SL | Inokuchi [30] |
| VH | Szeliski [53], Matusik [40], Tarini [55] |

Table 3.1: Selected algorithms from each class of algorithms

3.4 Class 1

In this section, we discuss techniques for reconstructing bright, textureless, and diffuse surfaces. The reconstruction of this type of surfaces is complicated by the fact that there is no spatial information available for stereo correspondence searching due to the lack of texture, thus making passive stereo based methods unavailable. Textureless and diffuse surface also indicates uniform reflectance, i.e., uniform diffuse albedo. The conditions under which each categories of algorithms would work or fail are listed in Table 3.2.

3.4.1 SfS

Shape from Shading, first proposed by Horn is targeted specifically for known isotropic Lambertian surfaces. By assuming orthographic projection, and known light source intensity and direction, surface orientation can be estimated from the shading variations.

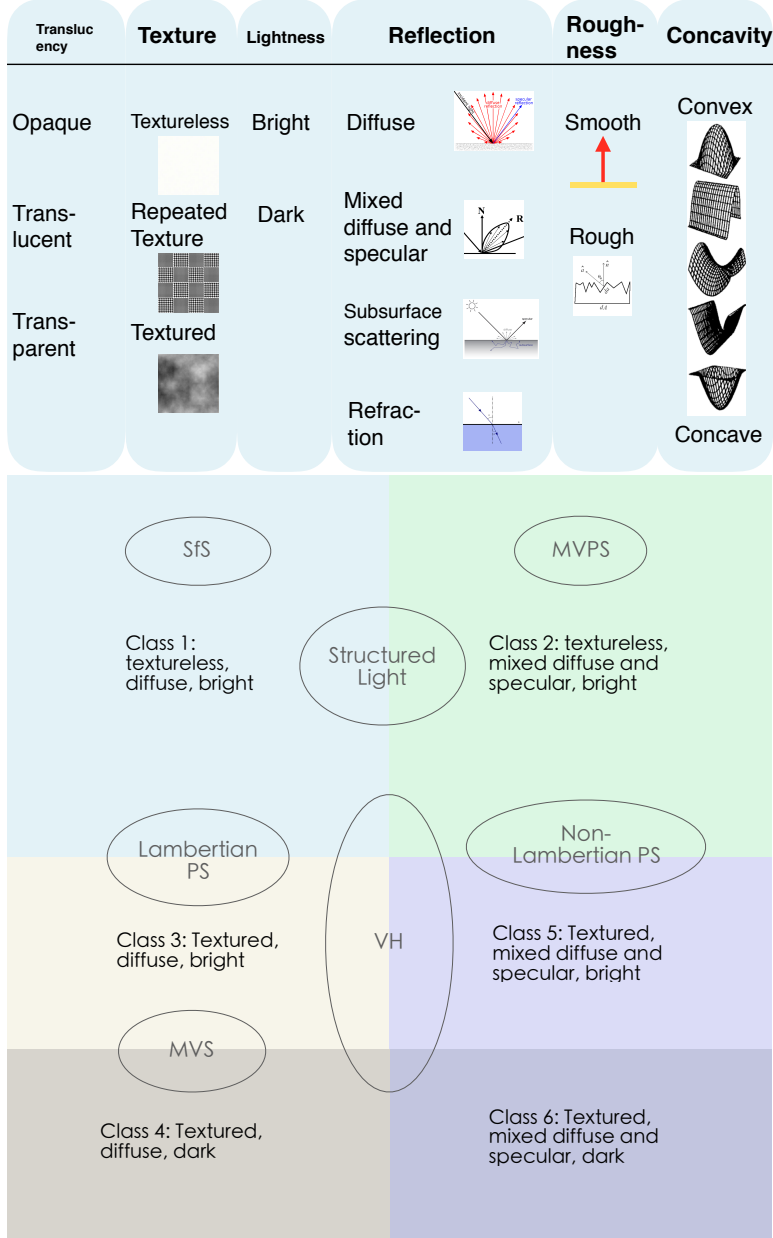


Figure 3.1: Top: A list of properties for object classes. Bottom: Six object classes of interest. Only texture, lightness, and reflectance are considered. Properties not considered are set as follows: opaque, rough (for Lambertian)/smooth (for Non-Lambertian), low concavity.

| Technique | Textureless | Bright | Lambertian |
|-------------------|-------------|--------|------------|
| SfS | ✓ | ✓ | ✓ |
| MVS | ✗ | ✓ | ✓ |
| Lamberian PS | ✓ | ✓ | ✓ |
| Non Lambertian PS | ✓ | ✓ | ✗ |
| MVPS | ✓ | ✓ | ✓ |
| SL | ✓ | ✓ | ✓ |
| VH | ✓ | ✓ | ✓ |

Table 3.2: Categories of algorithm that are applicable for object class 1.

3.4.2 Lambertian PS: uniform reflectance

The traditional Photometric Stereo can be considered as an extenstion of the original Shape from Shading, which incorporates additional light sources to eliminate ambiguity [61]. The surface orientation can be retrieved from using only two images.

To avoid the tedious process of light calibration, Silver [52] proposed a look-up scheme that relies on reflectance object with the same reflectance as the target, a uniform Lambertian surface in this case. This approach can be applied to surface with non-Lambertian reflectance, and varying colour or material, see Section 3.5 for non-Lambertian surfaces, and Section 3.7, 3.8 for surfaces with varying colour-/material.

3.4.3 SL

For stereo correspondence based methods, actively projected patterns have to be used for the lack of surface texture. Since the surface is diffuse, there is no specular reflection to cause severe noise.

3.5 Class 2

This section discusses the reconstruction of bright, textureless, non-Lambertian surfaces. The specular surfaces reflect light in a single direction which follows the law of reflection, thus the appearance changes as the viewpoint changes, which makes the correspondence search in these regions unreliable. Thus textureless and

non-Lambertian properties rule out stereo based techniques. Textureless also indicates that the surface is composed of the same material thus the albedo is uniform across the surface. The conditions under which each categories of algorithms would work or fail are listed in Table 3.3.

| Technique | Textureless | Bright | Non-Lambertian |
|-------------------|-------------|--------|----------------|
| SfS | ✓ | ✓ | ✗ |
| MVS | ✗ | ✓ | ✗ |
| Lambertian PS | ✓ | ✓ | ✗ |
| Non-Lambertian PS | ✓ | ✓ | ✓ |
| MVPS | ✓ | ✓ | ✓ |
| SL | ✓ | ✓ | ✗ |
| VH | ✓ | ✓ | ✓ |

Table 3.3: Categories of algorithm that are applicable for object class 2.

3.5.1 Non-Lambertian PS: uniform reflectance

This section considers techniques that deal with surfaces composed of the same material, i.e., *uniform albedo*. Techniques that can deal with spatially varying reflectance can generally be adapted to deal with surfaces of uniform reflectance. Thus refer to Section 3.8 for more techniques that are designed for surfaces of spatially-varying reflectance.

As discussed briefly in Section 3.4, we can also use a non-Lambertian *reference objects*. The method is first proposed by Silver and later by Hertzmann and Seitz.

3.6 Class 3

This section deals with bright, textured, Lamberian surfaces. Multi-view stereo can use the Lambertian, textured surface to reconstruct a (quasi-)dense model. The conditions under which each categories of algorithms would work or fail are listed in Table 3.4.

| Technique | Textured | Bright | Lambertian |
|-------------------|----------|--------|------------|
| SfS | ✗ | ✓ | ✓ |
| MVS | ✓ | ✓ | ✓ |
| Lamberian PS | ✓ | ✓ | ✓ |
| Non Lambertian PS | ✓ | ✓ | ✗ |
| MVPS | ✗ | ✓ | ✓ |
| SL | ✗ | ✓ | ✓ |
| VH | ✓ | ✓ | ✓ |

Table 3.4: Categories of algorithm that are applicable for object class 3.

3.6.1 MVS

The diffuse and textured surface is most suitable for MVS algorithms. However, active technique could work, but the surface texture might interfere with the encoding process thus making the reconstruction inaccurate. Furukawa use wide-baseline stereo matching to recover the 3D coordinates of salient feature points, then shrink a visual hull model so that the recovered points lie on its surface, then refine the result using energy minimization. Goesele et al. compute a depth map from each camera viewpoint (similar to [31]) and merge the results using VRIP [62]. Esteban and Schmitt first compute a depth map from each camera viewpoint and merge the results into a cost volume. They then iteratively deform a mesh, initialized at the visual hull, to find a minimum cost surface in this volume, also incorporating terms to fit silhouettes. Kolmogorov and Zabih [35] compute a set of depth maps using multi-baseline stereo with graph cuts, then merge the results into a voxel volume by computing the intersections of the occluded volumes from each viewpoint. Faugeras and Keriven compute a minimum cost surface by evolving a surface in a level-set frame-work, using a prediction-error measure. Vogiatzis et al. compute a correlation cost volume in the neighborhood of the visual hull. A minimum-cost surface is then computed using volumetric min-cut.

3.6.2 Lambertian PS: non-uniform reflectance

Visual texture can be thought of as a pattern or variance of intensity appearing on an object’s surface. In this thesis, the visual texture will be considered as resulting from non-uniform surface albedo. This section discusses techniques that deal with

surfaces of *spatially varying albedo*.

The original photometric stereo can also be used for surfaces with spatially-varying albedo. The albedo-scaled normal can be first estimated as usual, then the albedo is retrieved as the magnitude of the scaled normal [61]. This method requires three instead of two images.

To avoid the tedious process of light calibration, *uncalibrated photometric stereo* has been proposed. One approach used six or more pixels with the same albedo, and was able to solve for normals up to a rotation ambiguity[25]. It can be further proved that a 3-parameter subset of these transformations, known as the Generalized Bas-Relief (GBR) ambiguity, preserve surface integrability [10]. Thus, given three or more images of a Lambertian object acquired under light sources of unknown direction and strength, the surface can be reconstructed up to GBR transformation by enforcing surface integrability, see Figure 3.2 for the effect of GBR-ambiguity.

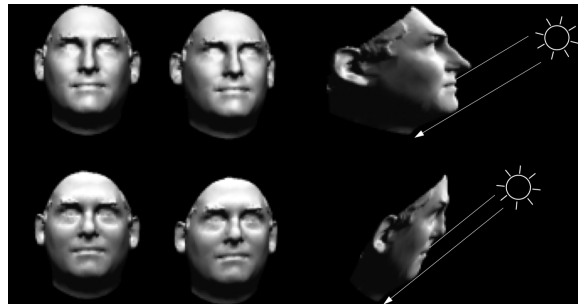


Figure 3.2: The effect of GBR ambiguity

The *reference object* approach, first proposed by Silver, and later revisited by in [26], can be used for surfaces with spatially varying reflectance. The basic assumption is that the BRDF at each point is a linear combination of the “basis” BRDFs defined by the set of reference objects.

3.7 Class 4

The dark surface, i.e., low reflectance makes any active lighting based technique unsuitable. Thus passive stereo based techniques still work in this case, see Section 3.6 for details.

| Technique | Textured | Dark | Lambertian |
|-------------------|----------|------|------------|
| SfS | ✗ | ✗ | ✓ |
| MVS | ✓ | ✓ | ✓ |
| Lamberian PS | ✓ | ✗ | ✓ |
| Non Lambertian PS | ✓ | ✗ | ✗ |
| MVPS | ✗ | ✗ | ✓ |
| SL | ✗ | ✗ | ✓ |
| VH | ✓ | ✓ | ✓ |

Table 3.5: Categories of algorithm that are applicable for object class 4.

3.8 Class 5

| Technique | Textured | Bright | Non-Lamberian |
|-------------------|----------|--------|---------------|
| SfS | ✗ | ✓ | ✗ |
| MVS | ✓ | ✓ | ✗ |
| Lamberian PS | ✓ | ✓ | ✗ |
| Non Lambertian PS | ✓ | ✓ | ✓ |
| MVPS | ✗ | ✓ | ✓ |
| SL | ✗ | ✓ | ✗ |
| VH | ✓ | ✓ | ✓ |

Table 3.6: Categories of algorithm that are applicable for object class 5.

3.8.1 Non-Lambertian PS: non-uniform reflectance

One approach exploits the fact that the reflectance of non-Lambertian surfaces can be approximated by **diffuse component and specular lobe**. Coleman and Jain and Barsky and Petrou who treat specular pixels as outliers, and Schluns, Sato and Ikeuchi, and Mallick et al. who assume the color of the specular lobe differs from the color of the diffuse lobe, allowing separation of the specular and diffuse components.

Due to the high complexity of the BRDF, some methods utilize analytical reflectance models. Goldman et al. uses an isotropic Ward model for each basis BRDF, and the surface orientation and parameters of the reflectance models are estimated iteratively. Alldrin et al. proposed a data-driven approach that got rid of

the parametric reflectance model, and employed a novel bi-variate approximation of isotropic reflectance functions. By combining this approximation with the weighted basis BRDFs, a per-pixel surface normal, global set of non-parametric basis BRDFs, and the corresponding weights are able to be independently estimated. Though the parametric reflectance model can significantly reduce the complexity of BRDFs, they are typically restricted to a limited classes of materials.

Another alternative to using BRDF models is to take advantage of the properties of BRDFs, include energy conservation, non-negativity, Helmholtz reciprocity, or isotropy. Helmholtz stereopsis introduced by Zickler et al. exploits the reciprocity to obtain the surface reconstruction. Isotropy is another physical property which holds for material without “grain”. Tan et al. use both symmetry and reciprocity present in isotropic BRDFs to resolve the generalized bas-relief ambiguity. Alldrin and Kriegman show that isotropy, with no further assumptions on surface shape or BRDF, can be utilized to recover the surface normal at each surface point up to a plane.

3.9 Class 6

We discuss textured, mixed diffuse and specular, and bright surface, which is challenging for MVS due to the specular nature, and is difficult for any active techniques since the low amount of reflected light.

| Technique | Textured | Dark | Non-Lamberian |
|-------------------|----------|------|---------------|
| SfS | ✗ | ✗ | ✗ |
| MVS | ✓ | ✓ | ✗ |
| Lamberian PS | ✓ | ✗ | ✗ |
| Non Lambertian PS | ✓ | ✗ | ✓ |
| MVPS | ✓ | ✗ | ✓ |
| SL | ✗ | ✗ | ✗ |
| VH | ✓ | ✓ | ✓ |

Table 3.7: Categories of algorithm that are applicable for object class 6.

3.9.1 VH

The non-Lambertian property makes any stereo based methods unavailable while the dark surface, or low reflectance makes active lighting methods unsuitable. Thus only visual hull fits in this case, the summary of VH algorithms are listed in Table 3.7.

| Technique | Representation | Algorithm |
|---------------|----------------|--------------------------|
| Szeliski [53] | 3D grids | Voxel-based |
| Tarini [55] | 3D rays | MI-based |
| Matusik [40] | Polygonal mesh | Exact polyhedral methods |

Table 3.8: Summary of VH representations and reconstruction approach.

3.10 Summary

Our taxonomy focuses on the visual cues detected in images, which is utilized by various techniques. Conceptualize these visual cues as dimension of the 3D reconstruction problem, we have an abstraction which allow us to think of algorithms as volumes within a n -dimensional problem space. Existing algorithms can be introduced into this framework based on the main visual cue used for reconstruction. Instances where these algorithms have been reported as supporting other forms of variation have been outlined, providing an initial mapping of the space that is summarized below in Table 3.9.

| Technique | Translucency | Texture | Lightness | Reflectance | Roughness | Concavity | Class |
|------------------|--------------|-------------|-----------|----------------|-----------|-----------|------------------|
| Horn [28] | Opaque | Textureless | Bright | Lambertian | N/A | Convex | Class 1 |
| Woodham [61] | Opaque | N/A | Bright | Lambertian | N/A | Convex | Class 1, 3 |
| Hayakawa [25] | Opaque | N/A | Bright | Lambertian | N/A | Convex | Class 1, 3 |
| Belhumeur [10] | Opaque | N/A | Bright | Lambertian | N/A | Convex | Class 1, 3 |
| Coleman [16] | Opaque | N/A | Bright | Non-Lambertian | N/A | Convex | Class 2, 5 |
| Barsky [9] | Opaque | N/A | Bright | Non-Lambertian | N/A | Convex | Class 2, 5 |
| Schluns [48] | Opaque | N/A | Bright | Non-Lambertian | N/A | Convex | Class 2, 5 |
| Sato [47] | Opaque | N/A | Bright | Non-Lambertian | N/A | Convex | Class 2, 5 |
| Mallick [37] | Opaque | N/A | Bright | Non-Lambertian | N/A | Convex | Class 2, 5 |
| Alldrain [5] | Opaque | N/A | Bright | Non-Lambertian | N/A | Convex | Class 2, 5 |
| Goldman [24] | Opaque | N/A | Bright | Non-Lambertian | N/A | Convex | Class 2, 5 |
| Silver [52] | Opaque | N/A | Bright | Non-Lambertian | N/A | Convex | Class 1, 2 |
| Hertzmann [26] | Opaque | N/A | Bright | Non-Lambertian | N/A | Convex | Class 1, 2, 3, 5 |
| Zickler [63] | Opaque | N/A | Bright | Non-Lambertian | N/A | Convex | Class 3, 5 |
| Furukawa [20] | Opaque | Textured | N/A | Lambertian | N/A | Convex | Class 3, 4 |
| Goesele [23] | Opaque | Textured | N/A | Lambertian | N/A | Convex | Class 3, 4 |
| Vogiatzis [59] | Opaque | Textured | N/A | Lambertian | N/A | Convex | Class 3, 4 |
| Szeliski [53] | Opaque | N/A | N/A | N/A | N/A | Convex | Class 1-6 |
| Tarini [55] | Opaque | N/A | N/A | N/A | N/A | Convex | Class 1-6 |
| Matusik [40] | Opaque | N/A | N/A | N/A | N/A | Convex | Class 1-6 |

Table 3.9: Algorithm classification based on the new taxonomy

Chapter 4

A Description of 3D Reconstruction

In Chapter 3, we introduce a taxonomy of 3D reconstruction which maps algorithms according to the visual/geometric characteristics of the object. However, without a formal ‘language’, i.e., a model and representations, the mapping from an algorithm to a column of the problem space would be largely empirical. Without a formal definition of the problem space, expressing the condition that an algorithm works well is not a well defined problem.

Computer vision problems require, among other factors, a model of the problem domain [36]. The relevant properties of the elements in the domain must be characterized and their relations must be analyzed. Representations describe the object properties selected by the model to facilitate solution of the problem. For instance, surface orientation is a geometric model, and surface normal or curvature are representations of this model. More specifically in the case of reconstruction problem, we first need to establish a model that defines the problem domain, then properties of the objects and surfaces are investigated to see their influence on the problem domain, which serves as the representation of the reconstruction problem.

In this chapter, we attempt to extend this taxonomy by providing a description of 3D reconstruction problem which allows for a well defined specification of the visual cues surrounding the problem and of the range of the desired solution, abstracting away from the functional specification of *how* to estimate a recon-

struction. We first propose a formal definition of the 3D reconstruction problem in Section 4.1. Section 4.2 discusses various key *aspects* of the problem space that are crucial to describe the appearance of the object. Section 4.3 the actual concrete representations of the proposed model. Section 4.4 provides examples of expressing common 3D reconstruction problems using the proposed model and representations. These four layers: Definition, Representation, Model, and Expression represent our framework of accessible 3D reconstruction.

4.1 Definition

We first give the definitions of some basic concepts, which include general computer vision concepts such as scene, camera, and image. We then define some other notions that are close related to the reconstruction problem before a formal definition is introduced. We then provide some reasonable approximations for a more practical definition.

4.1.1 Basic notations

We use the following notations: $\{C_n\}_{n=0}^{N-1}$ represents the camera set, which include both the intrinsic and extrinsic parameters; $\{I_n\}_{n=0}^{N-1}$ represents the set of all images; $\{L_n\}_{n=0}^{N-1}$ represents the set of light sources.

Definition 1 (Scene) The scene S is the four-dimensional joint spatio-temporal target of interest.

Definition 2 (Image) The 2D observation of the 3D scene S on the image plane of camera C_i at time t_0 , which is modelled as: $I_i = T(S, C_i, L_0, t_0)$, or on the image plane of C_0 under the light source L_i at time t_i , $I_i = T(S, C_0, L_i, t_i)$, where T is the geometric/radiometric transformation.

The transformation T can be a geometric one which determines the 2D coordinates of a 3D point, or a radiometric one which determines the intensity/irradiance information from the information of illumination, viewing direction and surface orientation, or both.

4.1.2 Segment and Scell

Definition 3 (Segment) A segment is a distinct region in the image.

Segment is the most basic element in the image, can be considered as a generalized pixel. For instance, a segment can be a pixel, a window area, an edge, a contour, or a region of arbitrary size and shape.

Definition 4 (Cue) cues are the visual or geometric characteristics of the segments seg that can be used for reconstruction, denoted as $cue(seg)$.

For instance, the cue can be texture within a window area, intensity/colour value of a pixel, or object contour, etc.

Definition (scell) A Scell (scene element) is a volume in the scene which corresponds to at least one segment.

A scell can be considered as a generalization of a voxel. However, a scell is not necessarily distinct since

Definition (Property) Properties are the visual and geometric characteristics of the Scell sc , which would influence the cues of a segment, denoted as $prop(sc)$.

The property of the scell can be the 3D position or orientation information, visual texture, reflectance, surface orientation, roughness, convexity, etc.

The relation between the notions define above is shown in Figure ??.

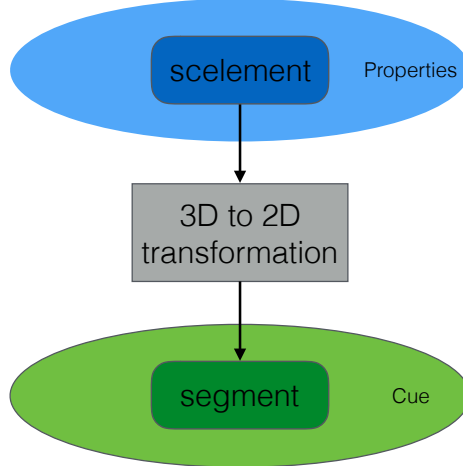


Figure 4.1: Relation between a scell and a segment

4.1.3 Photo-consistency

Every photograph of a 3D scene taken from a camera C_i partitions the set of all possible shape-radiance scene descriptions into two families, those that reproduce the photograph and those that do not. We characterize this constraint for a given shape and a given radiance assignment by the notion of *photo-consistency*.

Definition (Photo-consistency criterion) The photo-consistency criterion checks whether the properties of a scell sc can produce the cues observed in the corresponding segment seg .

$$consist(prop(sc), cue(seg)) = 1 \Rightarrow \text{photo consistent}$$

$$consist(prop(sc), cue(seg)) = 0 \Rightarrow \text{not photo consistent}$$

Definition (Segment photo-consistency) Let S be the scene. A scell $s \in S$ that is visible from C_i is photo-consistent with the image I_i if and only if the photo-consistency check is true.

Definition (Image photo-consistency) A scene S is image photo-consistent with image I_i if any scell $\forall s \in S$ visible from the camera C_i is segment photo-consistent with this image.

Definition (Scene photo-consistency) A scene S is scene photo-consistent with a set of images $\{I_n\}_{n=0}^{N-1}$ if it's image photo-consistency with each image $I_i \in \{I_n\}_{n=0}^{N-1}$ in the set.

4.1.4 Formal Definition

Definition (3D reconstruction) Given a set of images $\{I_n\}_{n=0}^{N-1}$ captured by cameras $\{C_n\}_{n=0}^{N-1}$, or under a set of light sources $\{L_n\}_{n=0}^{N-1}$, find a set of scells $\{sc_n\}_{n=0}^{M-1}$ such that any scell is photo-consistent with the image set $\{I_n\}_{n=0}^{N-1}$, i.e., $\forall sc_i \in \{sc_n\}_{n=0}^{M-1}$, we have $consist(prop(sc_i), cue(seg_{(i,n)})) = 1$.

where $seg_{(i,n)}$ is the corresponding segment of sc_i in camera C_n . Alternatively, 3D reconstruction tries to find a set of scelments $\{sc_n\}_{n=0}^{M-1}$ that are scene photo-consistent with the image set $\{I_n\}_{n=0}^{N-1}$

4.1.5 Applied Definition

While the definition presented above gives a formal definition of the problem of 3D reconstruction, it is not necessarily applicable in a practical setting. We extend in this section this formal definition to an approximate, but more applied version.

Definition (Photo-consistency score) The photo-consistency score measures the similarity between a scell sc and the corresponding segment seg .

$$\begin{aligned} consist(prop(sc), cue(seg)) &= x, x \in [0, 1] \\ consist(prop(sc), cue(seg)) &= 1 \Rightarrow \text{photo consistent} \\ consist(prop(sc), cue(seg)) &= 0 \Rightarrow \text{not photo consistent} \end{aligned}$$

Definition (Applied photo-consistency check) A scell sc and a segment seg are considered photo-consistent if the photo-consistency score is above a pre-defined threshold ε .

$$consist(prop(sc), cue(seg)) > \varepsilon$$

Some more definitions $\sum_{n \in I'} consist(prop(sc_i), cue(seg_{(i,n)}))$

Definition (Applied 3D Reconstruction) Given a set of images $\{I_n\}_{n=0}^{N-1}$ captured by cameras $\{C_n\}_{n=0}^{N-1}$, or under a set of light sources $\{L_n\}_{n=0}^{N-1}$, find a set of scells $\{sc_n\}_{n=0}^{M-1}$ such that the photo-consistency score between the set of scells and their corresponding segments $\{seg_{(i,n)}\}_{i=0, j=0}^{M-1, N-1}$ are maximized.

$$\text{maximize} \quad \sum_{n=0}^{N-1} \sum_{i=0}^{M-1} consist(rep(sc_i), prop(sc_i), cue(seg_{(i,n)}))$$

4.2 Model

Models and representations are fundamental for vision problem solving. Models select characteristic properties of an object, and representation describe object properties selected by the model to facilitate solution of a class of problem. A model facilitates the representation of aspects of reality useful in a particular problem domain [14]. For instance, surface orientation is one component of surface geometry model, and the corresponding representation can be surface normal or

curvature; another example is: colour is a component of material model, and RGB space is the corresponding representation of the colour.

We select the subset of the properties used for object taxonomy in Chapter 3 as the main components of our model. The model consisting of the key properties are shown in Table 4.2.

| Property | Texture | Lightness | Reflectance | Roughness | Concavity |
|----------|---------|-----------|-------------|-----------|-----------|
|----------|---------|-----------|-------------|-----------|-----------|

Table 4.1: Model of the 3D reconstruction problem: properties

In addition to the properties, there are requirements that can be imposed to the final reconstruction result. These requirements include but not exclude:

| Requirement | Accuracy-first | Completeness-first | Orientation-first | Roughness | Concavity |
|-------------|----------------|--------------------|-------------------|-----------|-----------|
|-------------|----------------|--------------------|-------------------|-----------|-----------|

Table 4.2: Model of the 3D reconstruction problem: requirements

4.3 Representation

Based on the proposed definitions and model of 3D reconstruction problem, we need to further define the representations so that 3D reconstruction problem can be expressed using the proposed model. Now we need to turn to how to represent the properties used in the proposed model, and these factors impact the corresponding properties.

4.3.1 Texture

Texture is one of the most important cues for many computer vision algorithms. It is generally divided into two categories, namely *tactile* and *visual* textures. Tactile textures refer to the immediate tangible feel of a surface whereas visual textures refer to the visual impression that textures produce to human observer, which are related to local spatial variations of simple stimuli like colour, orientation and intensity in an image. We focus only on visual textures as it's the most widely used ones in the stereo vision research, thus the term ‘texture’ thereafter is exclusively referred to ‘visual texture’ unless mentioned otherwise.

Although texture is an important component in computer vision, there is no precise definition of the notion texture. The main reason is that natural textures often exhibit different yet contradicting properties, such as regularity versus randomness, uniformity versus distortion, which can hardly be described in a unified manner.

There are various properties that make the texture distinguishable: scale/size-/granularity, orientation, homogeneity, randomness, and etc. However, due to the diverse and complexity of natural textures, it's a challenging task to map from these semantic meanings to the precise properties of a synthetic texture. The stereo vision community often take a simplified approach, classifying them into two categories: regular and stochastic ones by their degree of randomness. A regular texture is formed by regular tiling of easily identifiable elements (texels) organized into strong periodic patterns. A stochastic texture exhibits less noticeable elements and display rather random patterns. Most of the real world texture are mixtures of these two categories. We adopt another simplification and consider *texture coverage*, which is the ratio of the surface that is textured. Stereo vision, in theory, attempts to find the correspondences based on the ‘distinctiveness’ of the texture. Therefore, as long as the surface is covered by distinctive texture, it make little difference what the basic building texture element is.

4.3.2 Lightness

When light strikes a surface, it may be reflected, transmitted, absorbed, or scattered; usually, a combination of these effects occur. The intensity/colour information received by the sensor is thus determined, among other factors, the amount of light after these interaction. We consider intensity caused solely by reflection as it is the most common phenomenon and the easiest to analyse. Generally, we assume that all effects are local, thus global effects such as inter-reflection, transmission, and etc are omitted, which is called a **local interaction model**. Lightness ranges from ‘black’ to ‘white’ in the grey scale axis. Colour is a superset intensity, which takes account into the spectral composition of light. Both terms depend on illumination, surface normal, surface reflectance, and viewing direction.

In order to understand the contributing factor of pixel intensity/colour, we need

a in-depth understanding of reflection, i.e., how light is reflected off of a surface patch, and the relation between material and intensity value. The radiometric formation of an image consists of three separate process, *light-matter interaction*, *light-lens interaction*, and *light-sensor interaction*.

Definition of Radiometric Terms

Here is a list of radiometry terms, see Figure 4.2 for an illustration:

- Solid angle ($d\omega$): 3D counterpart of angle, $d\omega = \frac{dA \cos \theta_i}{R^2}$ (steradian).
- Projected solid angle ($d\Omega$): $d\Omega = \cos \theta d\omega$.
- Incident radiance ($\mathbf{L}_i(\theta_i, \phi_i)$): light flux received from the direction (θ_i, ϕ_i) on a unit surface area, unit ($\text{watt} \cdot \text{m}^{-2} \cdot \text{steradian}^{-1}$).
- Irradiance ($\mathbf{E}_i(\theta_i, \phi_i)$): light Flux (power) incident per unit surface area from all direction, $\mathbf{E}_i(\theta_i, \phi_i) = \int_{\Omega_i} L_i(\theta_i, \phi_i) d\Omega_i$ (watt/m^2).
- Surface radiance ($\mathbf{L}_r(\theta_r, \phi_r)$): light flux emmited from a unit surface area in the direction (θ_r, ϕ_r) , unit ($\text{watt} \cdot \text{m}^{-2} \cdot \text{steradian}^{-1}$).

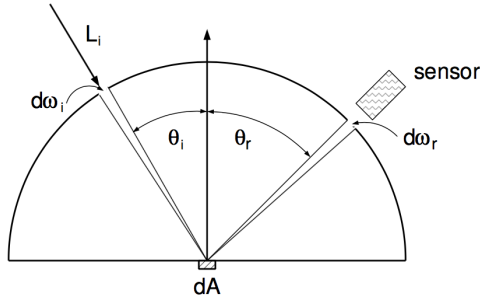


Figure 4.2: Light-matter interaction

Light-matter interaction

The relation between the incoming illumination and reflected light is model using the *bidirectional reflectance distribution function*, usually abbreviated BRDF. The BRDF is define as

Definition (BRDF) the ratio of the surface radiance $L_r(\theta_r, \phi_r)$ to the irradiance $E_i(\theta_i, \phi_i)$, i.e., $f(\theta_i, \phi_i, \theta_r, \phi_r) = \frac{E_{surface}(\theta_i, \phi_i)}{L_{surface}(\theta_r, \phi_r)}$.

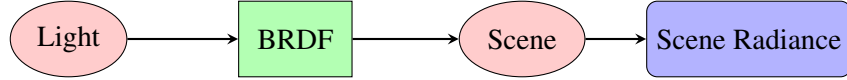


Figure 4.3: The light-matter interaction.

Diffuse Albedo or surface lightness is the proportion of incident light that is reflected by the surface. It should be noted that albedo is not an intrinsic property of a surface. Instead, for any surface, the albedo depends on the spectral and angular distributions of the incident light.

Light lens interaction

The assumption made in vision is that radiance is constant as it propagates along ray. Therefore the scene radiance is the same as the radiance hitting on the camera sensor. It can be further shown that the image irradiance received by the sensor is proportional to the scene radiance, thus the relation between *scene radiance* and *image irradiance* is linear.

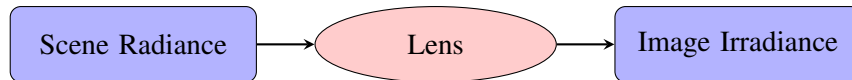


Figure 4.4: The light-lens interaction.

Light sensor interaction

The camera response function relating image irradiance at the image plane to the measured pixel intensity values is a non-linear mapping. A linear relation can be retrieved by radiometric calibration.

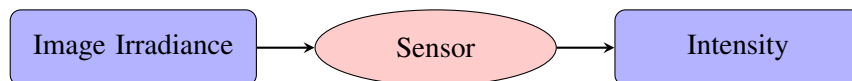


Figure 4.5: The light-sensor interaction.

In conclusion, if *light sensor* is assumed as a linear mapping as most of vision

algorithms do, or calibrated as a pre-processing step. The factor that influence the intensity is the BRDF value. There are 4 DoF for spatially-invariant BRDF, and for a special, simple case - Lambertian reflectance, the BRDF is degenerated to the diffuse *albedo*, which is the representation we adopt for intensity.

4.3.3 Reflectance

Specular surfaces reflect light in almost a single direction when the microscopic surface irregularities is small compared to light wavelength, and no subsurface scattering present [41]. Unlike diffuse reflections, which we experience the lightness and colour of an object, specular reflections carry information about the structure, intensity, and spectral content of the illumination field. In other words, specular reflection is simply image of the environment, or the illumination field, distorted by the geometry of the reflecting surface. See Figure 4.6, the image no long reflect the original colour of the surface (red), instead it shows a distorted image of the environment. A purely specular surface is a mirror. Purely specular surfaces are rare in nature. Most natural materials exhibit a mix of specular and diffuse reflection. Variations in microscopic surface geometry can cause specular reflections to be scattered, blurring the image of the environment in an amount proportional to surface roughness. We use a numeric *specularps* value to denote the proportion of specularity of the material, with 0 being completely diffuse, and 1 being completely specular or mirror light.

4.3.4 Roughness

Roughness, which is characterized as the microscopic shape characteristics of the surface, contributes to the way in which light is reflected off of a surface. A smooth surface may reflect incident light in a single direction, while a rough surface may scatter the light in various directions. We need prior knowledge of the microscopic surface irregularities, or a model of the surface to determine the reflection of incident light.

The possible surface models are divided into 2 categories: surface with exactly known profiles and surfaces with random irregularities. An exact profile may be determined by measuring the height at each point on the surface by means of a



Figure 4.6: A red specular sphere. The surface reflects light in a mirror-like way, and no diffuse reflection exist, thus the colour of the surface is no longer visible.

sensor such as the stylus profilometer. This method is cumbersome and impractical. Hence, it's more reasonable to model the surface as a random process, where it is described by a statistical distribution of either its height above a certain mean level, or its slope w.r.t its mean (macroscopic) slope. The section only discusses these second statistical approach.

Slope Distribution Model

We can think of a surface as a collection of planar micro-facets.

A large set of micro-facets constitutes an infinitesimal surface patch that has a mean surface orientation \vec{n} . Each micro-facet has its own orientation, which may deviate from the mean surface orientation by an angle α .

We will use the parameter α to represent the slope of individual facets. Surfaces can be modeled by a statistical distribution of the micro-facet slopes. If the surface is isotropic, the probability distribution of the micro-facet slopes can be assumed to be rotationally symmetric w.r.t the mean surface normal \vec{n} . Therefore, facet slopes can be described by a one-dimensional probability distribution function. For instance, the surface may be modeled by assuming a normal distribution

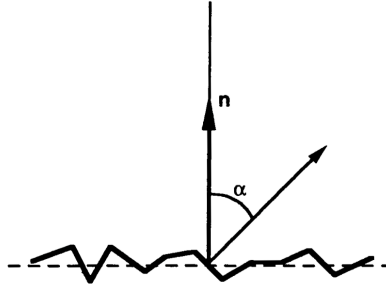


Figure 4.7: Surface Slope Distribution Model

for the facet slope α , with mean value $\bar{\alpha} = 0$ and standard deviation σ_α , and larger σ_α can be used to model rougher surfaces:

$$p_\alpha(\alpha) = \frac{1}{\sqrt{2\pi}\sigma_\alpha} e^{-\frac{\alpha^2}{2\sigma_\alpha^2}}$$

4.3.5 Concavity

Concavity can cause self-shadow or inter-reflection effect, which can severely impede the accuracy of intensity based algorithms. Since concavity is not shown in the silhouette image, methods that utilize silhouette information may also fail to reconstruct concavities. Concavity is measured by *surface curvature*.

4.4 Expression

Now with the proposed definition and representation of 3D reconstruction problem, we can express some existing 3D reconstruction algorithms under this framework. The expression of the reconstruction problem is shown in table 4.3.

| object | Texture coverage | Albedo | Specular | Roughness | Concavity |
|---------------|------------------|--------|----------|-----------|-----------|
| Class 1 | 0.2 | 0.8 | 0.2 | 0.8 | 0.2 |
| Class 2 | 0.2 | 0.8 | 0.5 | 0.2 | 0.2 |
| Class 3 | 0.8 | 0.8 | 0.2 | 0.8 | 0.2 |
| Class 5 | 0.8 | 0.8 | 0.5 | 0.2 | 0.2 |

Table 4.3: Expression of the reconstruction problem for the object class 1, 2, 3, 5.

Chapter 5

A Mapping of 3D Reconstruction

Most of the vision work focuses on developing algorithmic novelties, and very few investigates the rigorous conditions under which these algorithms work. Thus this knowledge is only known empirically, without a rigorous definition of the problem or application domain or the conditions. This section builds upon the 3D description proposed in Chapter 4, and attempts to find out the optimal algorithms under a pre-defined condition.

To achieve this goal, we need a dataset to evaluate the performance of each algorithm under varied conditions, which is not the goal of most of the online datasets. To the best of our knowledge, current existing 3D benchmarks focus on one specific class of algorithms, for example, the Middlebury dataset is targeted at MVS algorithms, and the ‘DiLiGenT’ dataset is for Photometric Stereo algorithms. This makes them only suitable to the evaluation of algorithms within the same category. There is no dataset that evaluates 3D reconstruction across differ categories, let alone one that covers a range of properties and their combinations. The reasons for the lack of such dataset is: 1). it’s already tedious to create a real-world dataset for a specific category of algorithms, it would be even more challenging to create a dataset for a larger range of algorithms with the ground truth; 2). it’s practically impossible to make one property, e.g., , noise level, lighting configuration, material, etc, varied while fixing the others in order to conduct a thorough evaluation.

We propose a synthetic but realistic (physically-based) dataset for evaluation of 3D reconstruction algorithms. The dataset includes a collection of images of

a scene under different material or lighting conditions. The camera/projector intrinsic and extrinsic parameters are computed directly from the configurations of the synthetic setup, and the ground truth, including the 3D model point cloud and normal map, are generated directly from Blender.

5.1 Synthetic setup

We use the physical-based renderer Cycles in Blender to generate the synthetic dataset. For each technique, the configuration of the camera remains fixed. The image resolution is 1280×720 , with a focal length of $35mm$ or $1400px$.

For MVS, there are five rings of cameras, of which the elevation angle is 15° , 30° , 45° , 60° , 90° . The between-angle of two neighbouring cameras is 30° , 30° , 45° , 45° , and 360° . Thus there are in total $12 + 12 + 8 + 8 + 1 = 41$ cameras.

For photometric stereo, according to [11], increasing the number of images is only important up to a point, the experimental results showed that most algorithms reaches to optimum when 15 images are used. To make a balance between algorithm performance and rendering time, we use 25 light sources, which are distributed on four different rings with elevation angle of 90° , 85° , 60° , and 45° . The azimuth angle between two neighbouring light sources is 45° .

For the structured light, the baseline angle between the camera and the projector is 10° , and only one camera is used, thus only a portion of the object is invisible. The resolution of the projector is 1024×768 , thus 10 Gray code patterns are needed. To counter the effect of inter-reflection, each pattern and its inverse are projected, which makes it less sensitive to scattered light.

5.2 Structure of Datasets

Due to the number of properties and number of levels for each property, it would be unrealistic to render all the combinations of properties. For if we have N properties and each is discretized into L levels, the number of different combinations is L^N , and for each combination, there are in total $41 + 25 + 42 = 108$ images to render. Therefore, we take another approach: 1). first we investigate the *dependency* between any two properties, if these two properties are independent, there is no need to render all their combinations whereas it's necessary to do so if they are

dependent; 2). render all the dependent properties and their combinations.

5.3 Selected methods

We have selected one representative algorithm from each class of algorithms: the PMVS proposed in [20], the example-based photometric stereo proposed in [26], and the Gray-encoded structured light technique. The current implementation of SL projects both column and row patterns, and depth values are computed using these two kinds of patterns individually. A depth consistency checking step is performed to reject erroneous triangulations.

5.4 Evaluation metrics

We use the metric proposed in [50] to evaluate MVS and SL algorithms. More specifically, we compute the accuracy and completeness of the reconstruction. For accuracy, the distance between the points in the reconstruction R and the nearest points on ground truth G is computed, and the distance d such that $X\%$ of the points on R are within distance d of G is considered as accuracy. Thus the lower the accuracy value, the better the reconstruction result. For completeness, we compute the distance from G to R . Intuitively, points on G is not “covered” if no suitable nearest points on R found. A more practical approach computes the fraction of points of G that are within an allowable distance d of R . Note that as the reconstruction gets better, the “accuracy value” goes down, but the “accuracy” is often claimed as improved, which is contradictory at first glance. To make it more consistent to the natural context, we say the accuracy goes up when the reconstruction gets better.

For photometric stereo, we employ another evaluation criteria, which is based on the statistics of angular error. For each pixel, the angular error is calculated as $\arccos(n_g^T n)$ in degrees, where n_g and n are the ground truth and estimated normals respectively. In addition to the mean angular error, we also calculate the minimum, maximum, median, the first quartile, and the third quartile of angular errors for each estimated normal map.

5.5 Dependency Check

Part of the difficulty in establishing a comprehensive set of experiments for such an evaluation is the large variability of shapes and material properties. We conduct a dependency check that evaluates the performance of the algorithm by changing two properties at a time while fixing the others. The goal is to identify the dependent properties so that the dimension of the problem domain could become more manageable.

5.5.1 PMVS

We evaluate the performance of PMVS in terms of accuracy and completeness under varied combinations of properties, the settings of the properties and all their combinations are listed in Table 5.1.

| Property | Texture | Albedo | Specular | Roughness |
|----------|------------|------------|------------|------------|
| (a) | [0.2, 0.8] | [0.2, 0.8] | 0.0 | 0.0 |
| (b) | [0.2, 0.8] | 0.8 | [0.2, 0.8] | 0.0 |
| (c) | [0.2, 0.8] | 0.8 | 0.0 | [0.2, 0.8] |
| (d) | 0.8 | [0.2, 0.8] | [0.2, 0.8] | 0.0 |
| (e) | 0.8 | [0.2, 0.8] | 0.0 | [0.2, 0.8] |
| (f) | 0.8 | 0.8 | [0.2, 0.8] | [0.2, 0.8] |

Table 5.1: Property settings of the pairwise conditions used for the dependency check of the MVS algorithms.

5.5.2 Property and Reconstruction

We investigate how each property affects the reconstruction in terms of accuracy and completeness.

(a), (b), (c) Texture As the texture level increases, the accuracy and completeness both increase. Thus texture has a positive correlation with the accuracy and completeness of the reconstruction.

(b), (d) Specular As the specular level goes up, the accuracy and completeness of the reconstruction gets worse. Thus specular has an negative correlation with the accuracy and completeness of the reconstruction. See Figure 5.2.

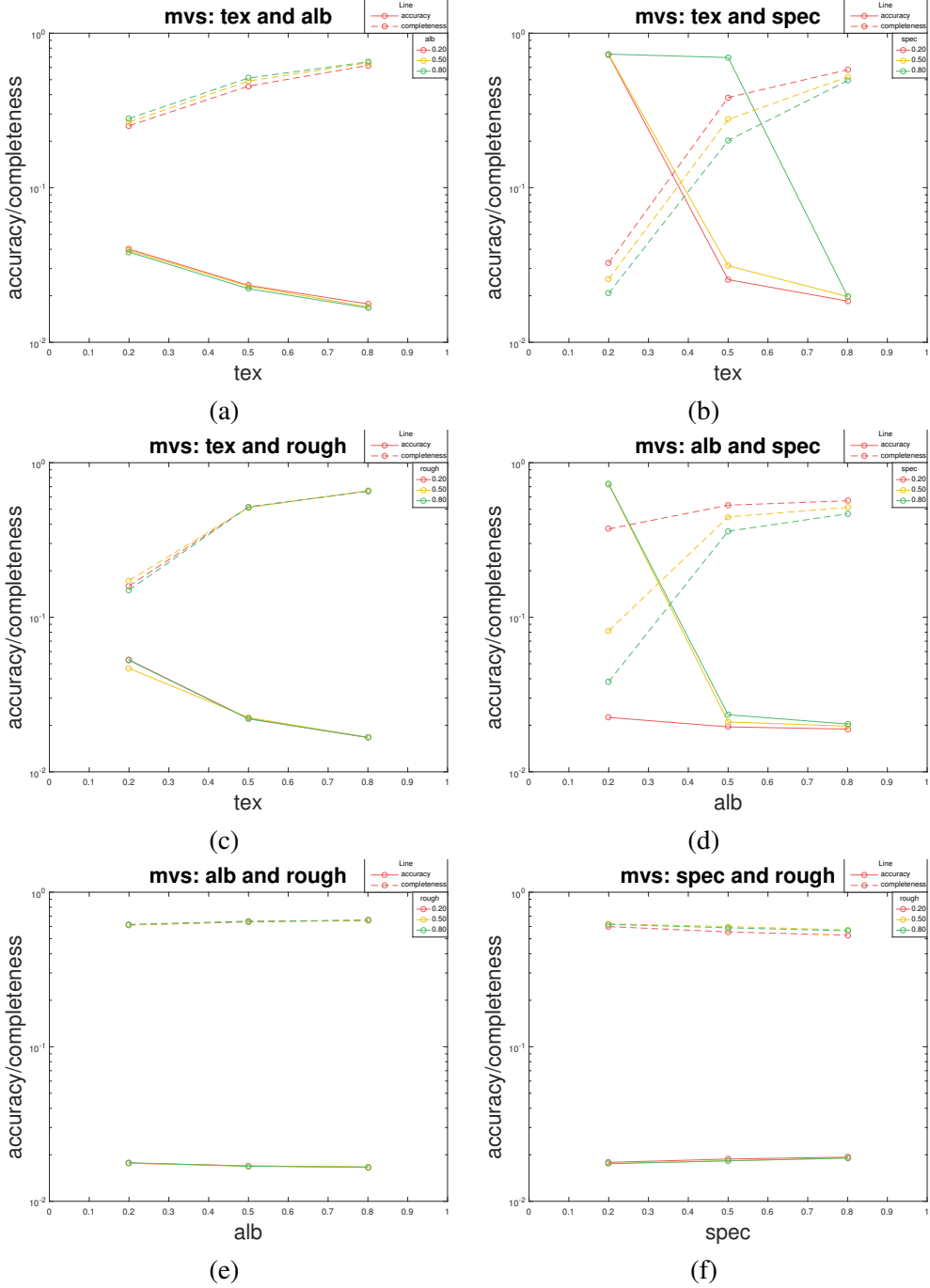


Figure 5.1: Performance of PMVS under six pairwise conditions. For instance, (a) shows the performance under changing *texture* and *albedo* values. The property values are assigned based on (a) of Table 5.1.

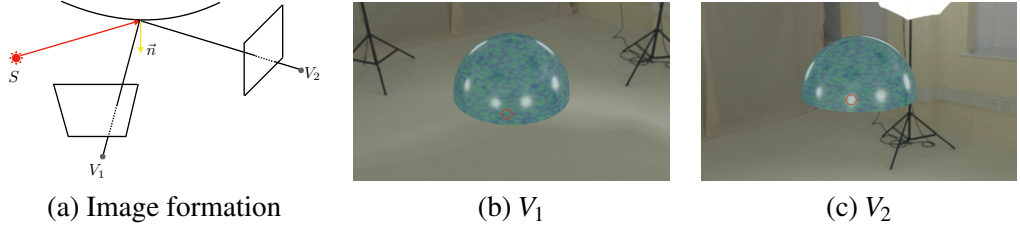


Figure 5.2: (a) shows the reflection of light off a specular surface. V_1 received the diffuse component while V_2 receives the specular component. (b), (c) shows the images observed from these two views. The specular area (red circle) observed in V_2 is visible in V_1 .

(b) Texture and Specular For a fixed texture, as the specularity goes up, the accuracy and the completeness goes up, which is consistent to previous observations. Besides, for a lower value texture, the effect of specular is more substantial than that for a higher value texture. However, we observe that, the specular has a bigger impact on lower textured surface, this can be explained as: the specular lobe is observed only by cameras positioned and oriented towards the specular lobe, thus only a highlight is visible, as shown in Figure 5.2 V_2 . Thus cameras positioned otherwise would observe the true surface, as shown in Figure 5.2 V_1 . The reconstruction exploits the texture information provided by views like V_1 , and thus is able to reconstruct the specular surfaces. If the surface texture level decreases, as shown before, the reconstruction deteriorates.

(d) Albedo and Specular For a fixed albedo, as the specular goes up, the accuracy and completeness both goes down, which is consistent to previous observations. However, the effect of specular is more substantial for a lower value albedo than that for a higher value albedo. See Figure 5.3.

(f) Specular and Roughness The effect of roughness is that it can diminish the specular and make the surface appear diffuse. Since specular has a negative impact on the reconstruction, in theory, roughness should have a positive impact on the reconstruction. However, since this test is conducted on highly textured surface, as discussed before, the reconstruction is still good for specular, highly textured surface, refer to 5.1(b). That's why the effect of roughness on specular seems insignificant. Since for this method, these two properties are closely related, we'll

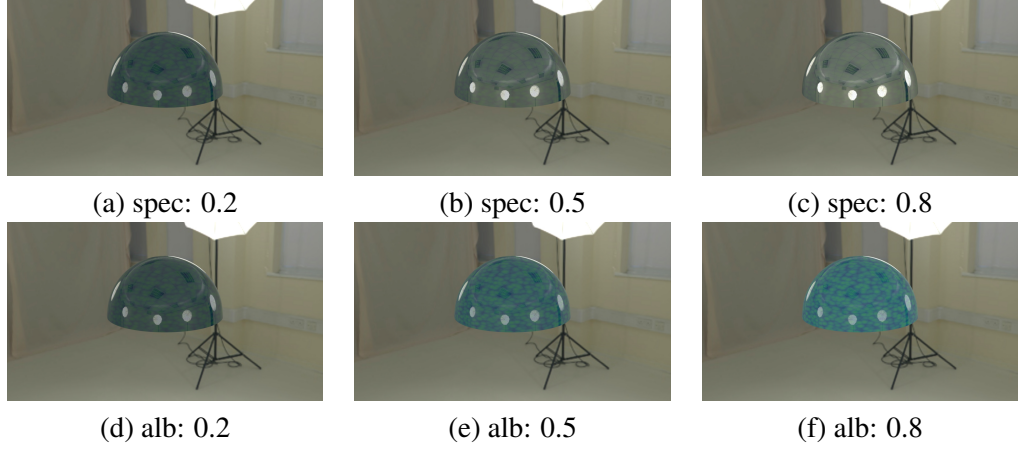


Figure 5.3: (a)-(c). The albedo is set as 0.2, (d)-(f). the specular is set as 0.2.

According to energy conservation, as the specular component increases, the diffuse component decreases.

just consider specular only, and ignore roughness. since a low specular achieve almost the same result as a high specular and rough surface, we would just combine these two factors into a single one, and consider the specular only for simplicity.

Conclusion The most important property is, high texture would lead to good reconstruction. Specular effect would deteriorate the reconstruction for lower textured and lower albedo surfaces. Since low specular and high specular + rough achieves almost the same results, we combine these two factors together and consider specular only.

the properties that have an effect on the MVS are: texture, albedo, and specularity, as shown in Table 5.2. Thus, we will only consider these three properties for all forthcoming discussion of MVS.

| Metric | Texture | Albedo | Specular | Roughness |
|--------------|---------|--------|----------|-----------|
| Accuracy | ✗ | ✓ | ✓ | ✗ |
| Completeness | ✓ | ✓ | ✓ | ✗ |

Table 5.2: The correlation between each property and the metrics *accuracy* and *completeness*.

5.5.3 Example-based PS

We evaluate the performance of example-based PS in terms of angular difference under varied combinations of properties. The statistical measures that we used include median, mean, first and third quartile of the angular difference. We investigate two properties at a time. The settings of the properties and all their combinations are listed in Table 5.3.

| Property | Texture | Albedo | Specular | Roughness |
|----------|------------|------------|------------|------------|
| (a) | [0.2, 0.8] | [0.2, 0.8] | 0.0 | 0.0 |
| (b) | [0.2, 0.8] | 0.8 | [0.2, 0.8] | 0.2 |
| (c) | [0.2, 0.8] | 0.8 | 0.0 | [0.2, 0.8] |
| (d) | 0.0 | [0.2, 0.8] | [0.2, 0.8] | 0.2 |
| (e) | 0.0 | [0.2, 0.8] | 0.0 | [0.2, 0.8] |
| (f) | 0.0 | 0.8 | [0.2, 0.8] | [0.2, 0.8] |

Table 5.3: Property settings of the pairwise conditions used for the dependency check of the Photometric Stereo algorithms.

5.5.4 Property and Reconstruction

We investigate how each property affects the reconstruction in terms of the statistics of the angular difference.

(a), (b), (c) Texture As the texture level increases, all statistic measures of the angular difference remain almost the same. Thus texture doesn't affect the reconstruction of the chosen PS algorithm.

(a), (d), (e) Albedo As the albedo level increases, all statistic measures of the angular difference decreases. Thus the albedo has a positive correlation to the reconstruction.

(b), (d), (f) Specular As the specular level goes up, all statistic measures of the angular difference increases. Thus specular has an negative impact on the reconstruction.

(c), (e), (f) Roughness The effect of roughness is a bit complicated. Generally, it will improve the reconstruction as the roughness goes higher. However, as shown in Figure 5.4 (f), the roughness will cause worse reconstruction for medium high value, which will be discussed more later. As the surface roughness increases, the

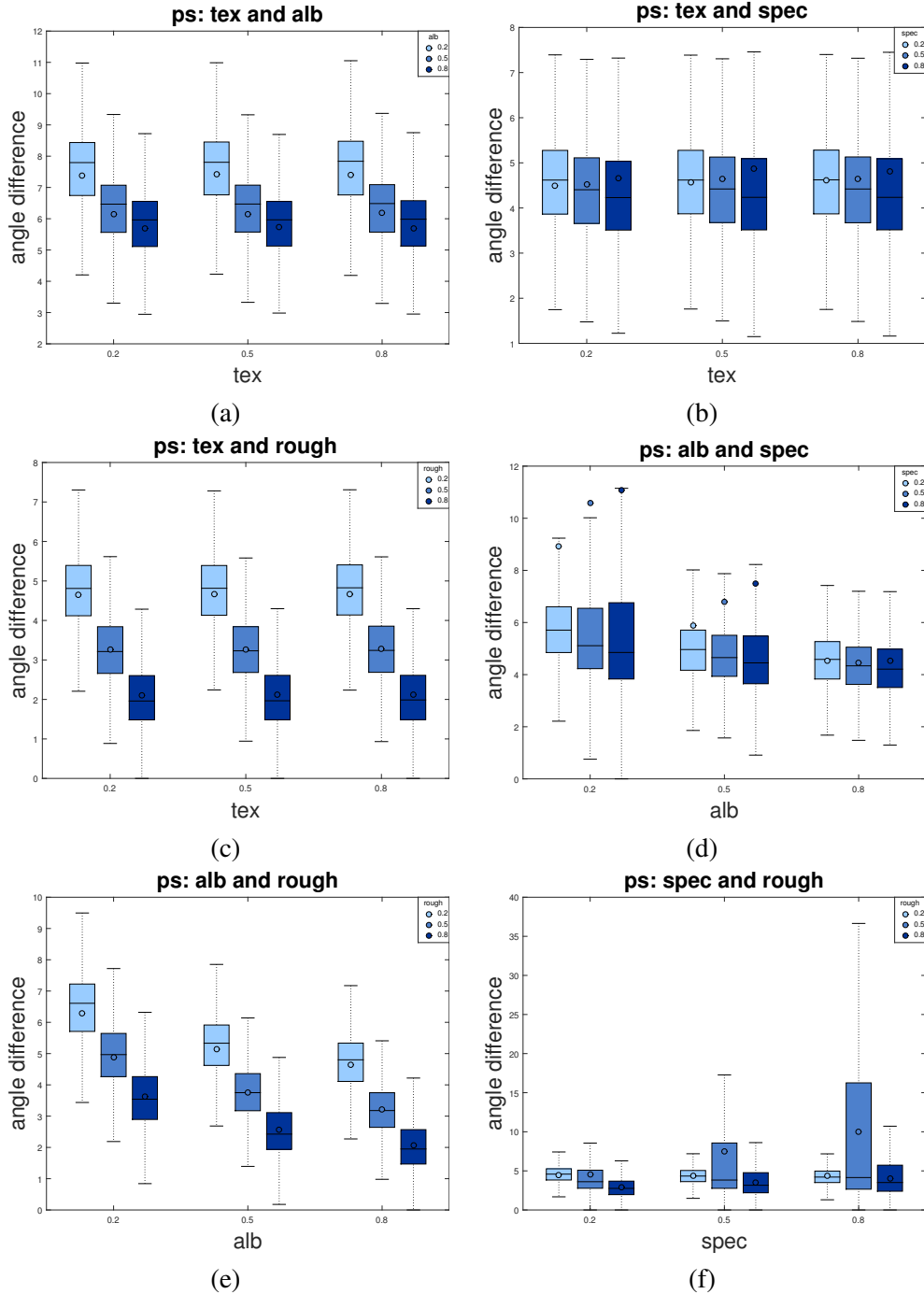


Figure 5.4: Performance of Example-based PS under six pairwise conditions.

For instance, (a) shows the performance under changing *texture* and *albedo* values. The property values are assigned based on Table 5.3 (a).

size of the highlight increases, making elimination of specularity harder. However, if the roughness increases enough, the surface begins to look diffuse.

(b) Texture and Specular For a fixed texture, as the specular increases, only the specular regions exhibit erroneous normal estimation, the rest of the surface is reliably estimated. That is why the median value is non-increasing while the mean value increases as is shown in Figure 5.4 (b), and Figure 5.5.

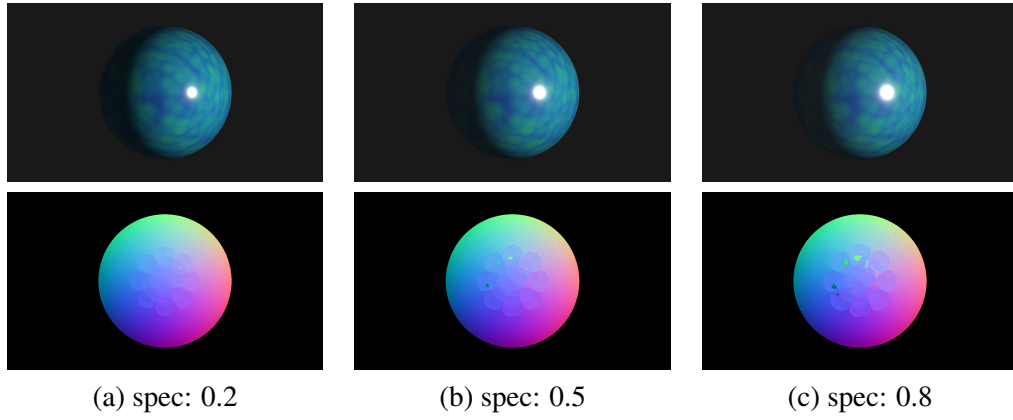


Figure 5.5: (a)-(c). The texture is set as 0.5. According to energy conservation, as the specular component increases, the diffuse component decreases.

(d) Albedo and Specular For a fixed albedo, as the specular level increases, the normal estimation of the specular areas gets worse while the rest of the surface are reliably estimated, see Figure 5.6 (a) - (c), and Figure 5.4 (d). For a fix specular, as the albedo level increases, the normal estimation of the specular areas gets better, see Figure 5.6 (d) - (f), and Figure 5.4 (d).

(f) Specular and Roughness For a fixed specularity, if the specularity is lower, the effect of roughness is less noticeable, whereas if the specularity is higher, the effect of roughness becomes more substantial. We've also noticed a ‘peculiar’ case when roughness is 0.5, it makes the reconstruction worse, which is counter-intuitive. However, we argue that it's because the roughness effect is not strong enough to cancel out the specularity, thus causing a much larger area of ‘blurred’ specularity, which makes the reconstruction worse. This effect is also demonstrated in the training stage, see Figure ?? for some visual examples.

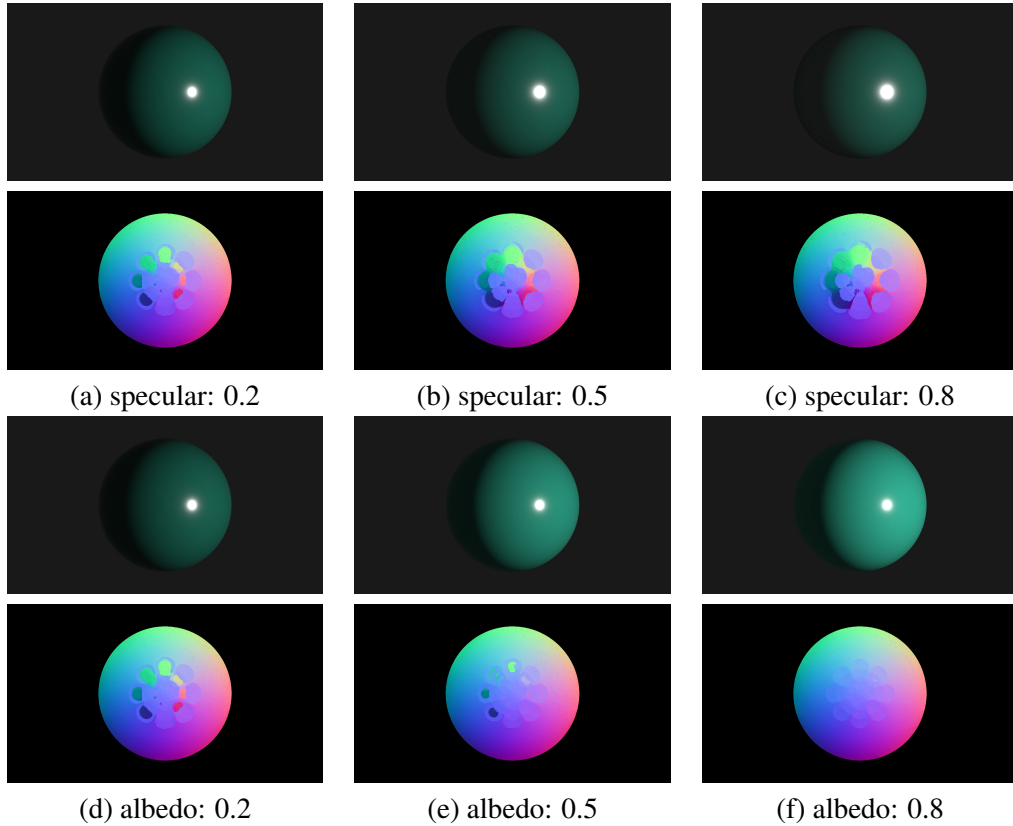


Figure 5.6: (a)-(c). The albedo is set as 0.2, (d)-(f). the specular is set as 0.2.

According to energy conservation, as the specular component increases, the diffuse component decreases.

Conclusion the properties that have an effect on the PS are: albedo, specularity, and roughness, as shown in Table 5.4. Therefore, we will only consider these three properties for all forthcoming discussion of PS.

| Metric | Texture | Albedo | Specular | Roughness |
|------------------|---------|--------|----------|-----------|
| Angle difference | ✗ | ✓ | ✓ | ✓ |

Table 5.4: The correlation between each property and the metric *angular difference*.

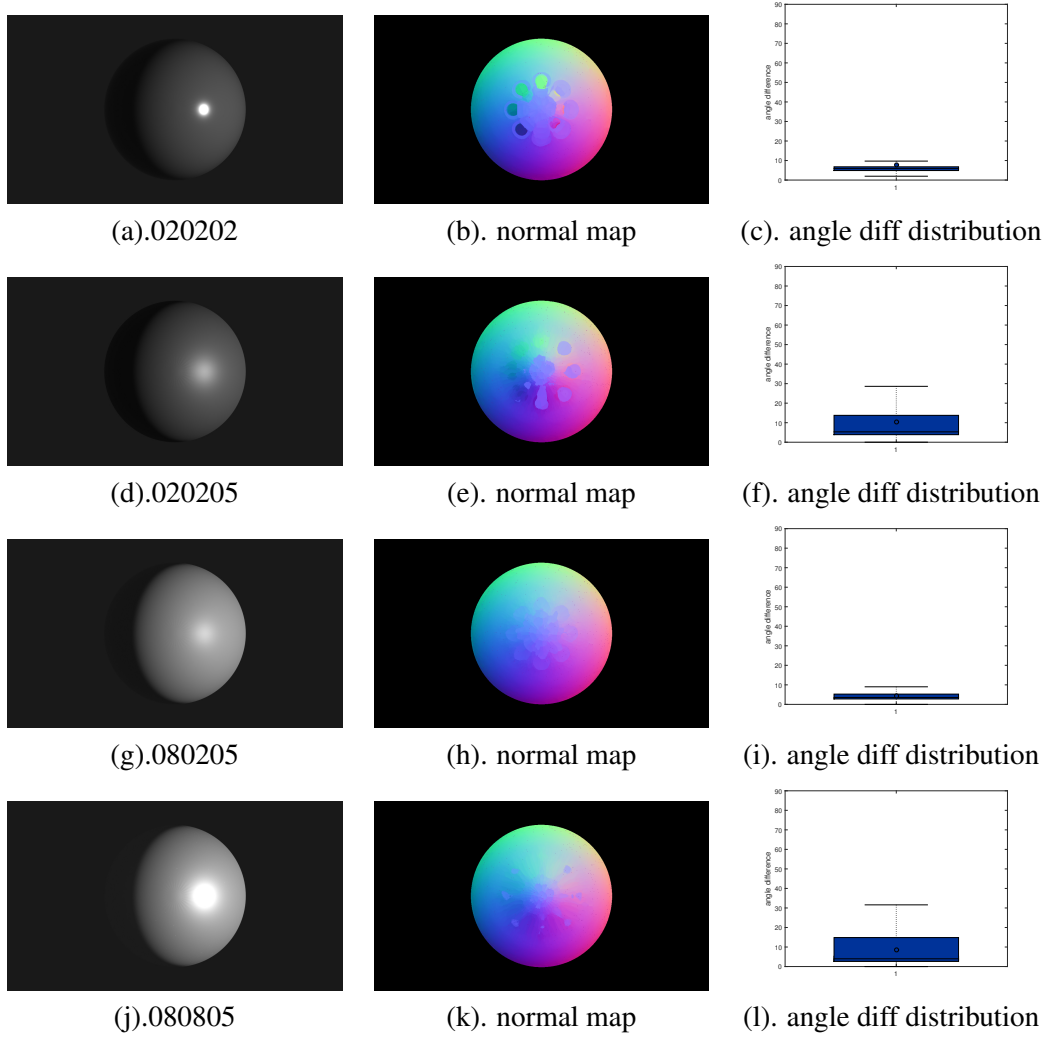


Figure 5.7: The ‘peculiar’ effect of roughness on PS. The order of the property is: albedo, specular, and roughness, thus 080205 means albedo: 0.8, specular: 0.2, and roughness: 0.5

5.5.5 Gray-code SL

We evaluate the performance of Gray-code SL in terms of accuracy and completeness under varied combination of properties, the settings of the properties and all their combinations are listed in Table 5.5.

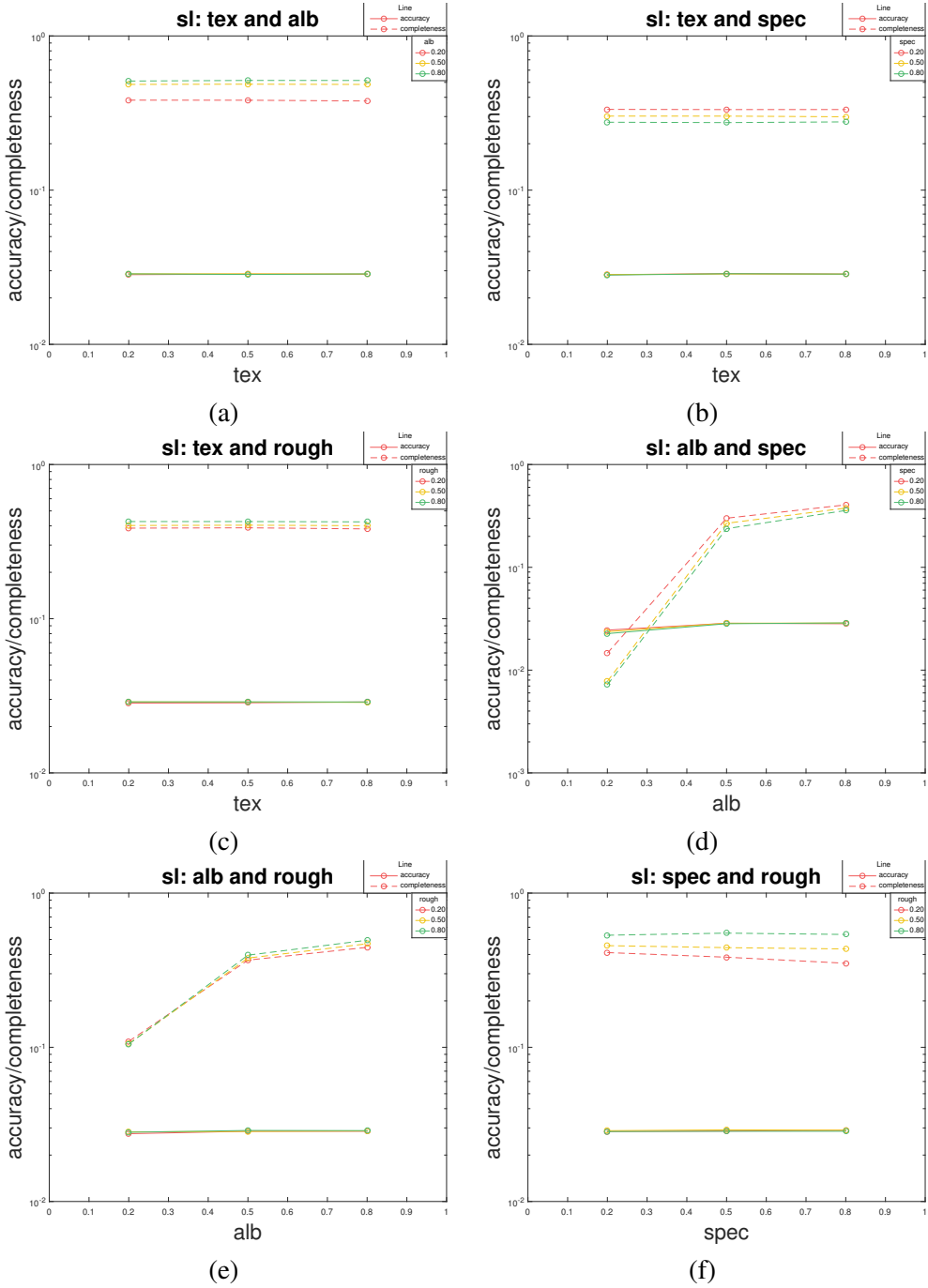


Figure 5.8: Performance of Gray-encoded SL under six pairwise conditions.

For instance, (a) shows the performance under changing *texture* and *albedo* values. The property values are assigned based on Table 5.5 (a).

| Property | Texture | Albedo | Specular | Roughness |
|----------|------------|------------|------------|------------|
| (a) | [0.2, 0.8] | [0.2, 0.8] | 0.0 | 0.0 |
| (b) | [0.2, 0.8] | 0.8 | [0.2, 0.8] | 0.0 |
| (c) | [0.2, 0.8] | 0.8 | 0.0 | [0.2, 0.8] |
| (d) | 0.0 | [0.2, 0.8] | [0.2, 0.8] | 0.0 |
| (e) | 0.0 | [0.2, 0.8] | 0.0 | [0.2, 0.8] |
| (f) | 0.0 | 0.8 | [0.2, 0.8] | [0.2, 0.8] |

Table 5.5: Property settings of the pairwise conditions used for the dependency check of the Structured Light algorithms.

5.5.6 Property and Reconstruction

We investigate how each property affects the reconstruction in terms of accuracy and completeness. A depth check step is performed to remove erroneous depth, thus the accuracy remain almost constant across all cases.

(a), (b), (c) Texture As the texture level increases, the accuracy and completeness remain almost constant. Thus texture doesn't affect the reconstruction of the chosen SL algorithm.

(a), (d), (e) Albedo As the albedo level increases, the accuracy remain almost constant while the completeness increases. Thus albedo has a positive correlation with completeness.

(b), (d), (f) Specular As the specular level goes up, the accuracy remain almost constant while the completeness of the reconstruction decreases. Thus specular has an negative correlation with the completeness of the reconstruction.

(c), (e), (f) Roughness As the roughness level increases, the accuracy remain almost constant while the completeness increases. Thus roughness has a positive correlation with completeness.

(d) Albedo and Specularity For a fixed albedo, the completeness goes down as the specularity goes up for low albedo surface, see Figure 5.9 (a)-(c). This effect becomes less substantial when the albedo increases. For a fixed specular, the completeness goes up as the albedo increases, see Figure 5.9 (d)-(f). Thus we conclude that the effect of specular is most significant when the albedo is low. See Figure 5.9 (d).

(f) Specular and Roughness For a fixed roughness, as the specular increases,

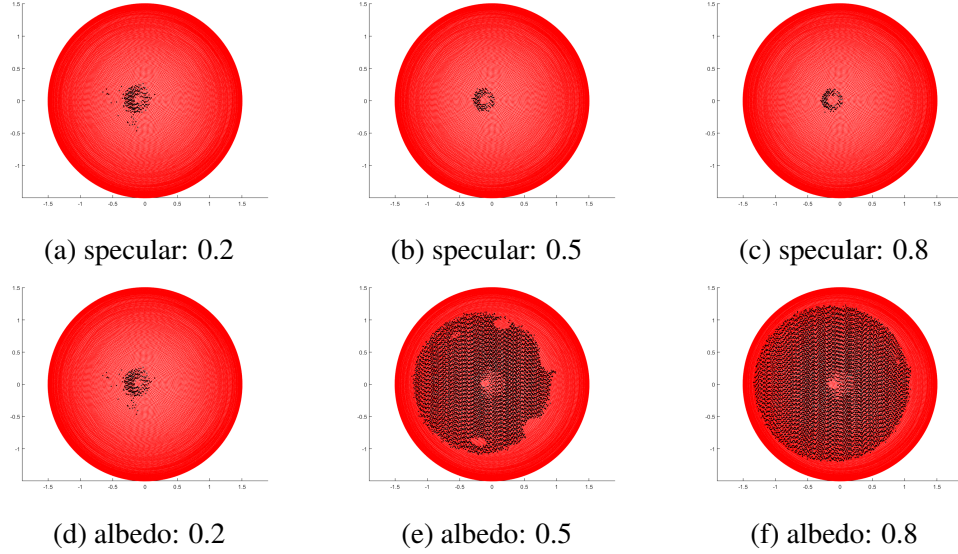


Figure 5.9: (a)-(c). The albedo is set as 0.2, (d)-(e). the specular is set as 0.2.

According to energy conservation, as the specular component increases, the diffuse component decreases.

the completeness decreases, see Figure 5.10. For a fixed specular, as the roughness goes up, the completeness increases, see Figure 5.10 (d)-(f).

Conclusion the properties that have an effect on the SL are: texture, albedo, specularity, as shown in Table. Therefore, we will only consider these three properties for all forthcoming discussion of SL.

| Metric | Texture | Albedo | Specular | Roughness |
|--------------|---------|--------|----------|-----------|
| Accuracy | ✗ | ✗ | ✗ | ✗ |
| Completeness | ✗ | ✓ | ✓ | ✓ |

Table 5.6: The correlation between each property and the metrics *accuracy* and *completeness*.

5.6 Training

For each technique, we generate the synthetic dataset using only the dependent properties, thus there are $L \times L \times L$ different combinations for each technique,

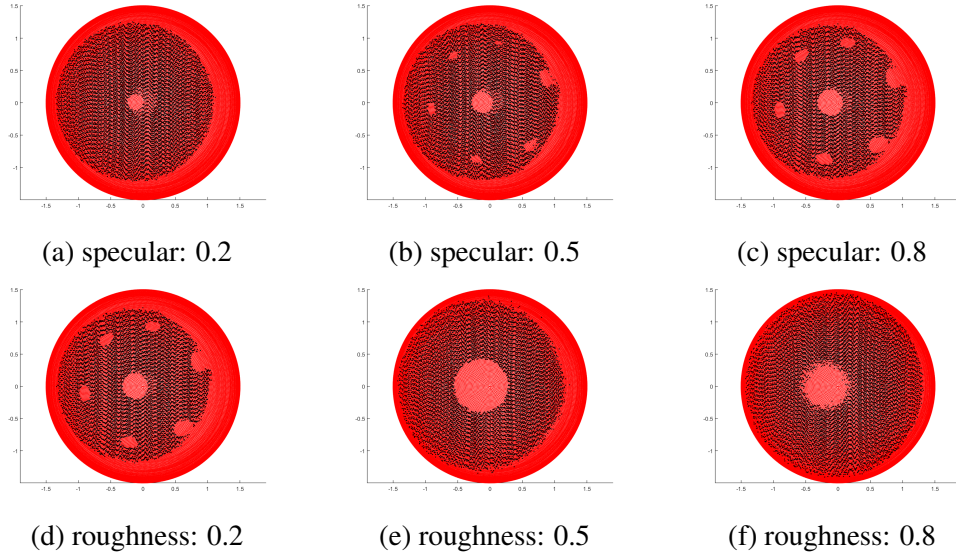


Figure 5.10: (a)-(c). The roughness is set as 0.2, (d)-(e). the specular is set as 0.8. According to energy conservation, as the specular component increases, the diffuse component decreases.

where L is the number of levels for each property.

5.6.1 PMVS

The performance of PMVS under different combinations of properties is shown in Figure 5.11. The conditions that PMVS works well is listed in Table ??.

We make the following observations from the training results

- (a)-(c): albedo could counteract the effect of specular, take the case when $\text{tex} = 0.5$ as an example, as the albedo increases, the result becomes better. The effect albedo has on specular has to do with surface texture, i.e., higher texture, more significant the influence is.
- (d)-(f): specular has a bigger impact on low texture surfaces than on high texture ones, i.e., for low textured surface, even low specular would result in bad results whereas for high textured surface, satisfactory results could be achieved under high specular cases. This is illustrated in Figure 5.2

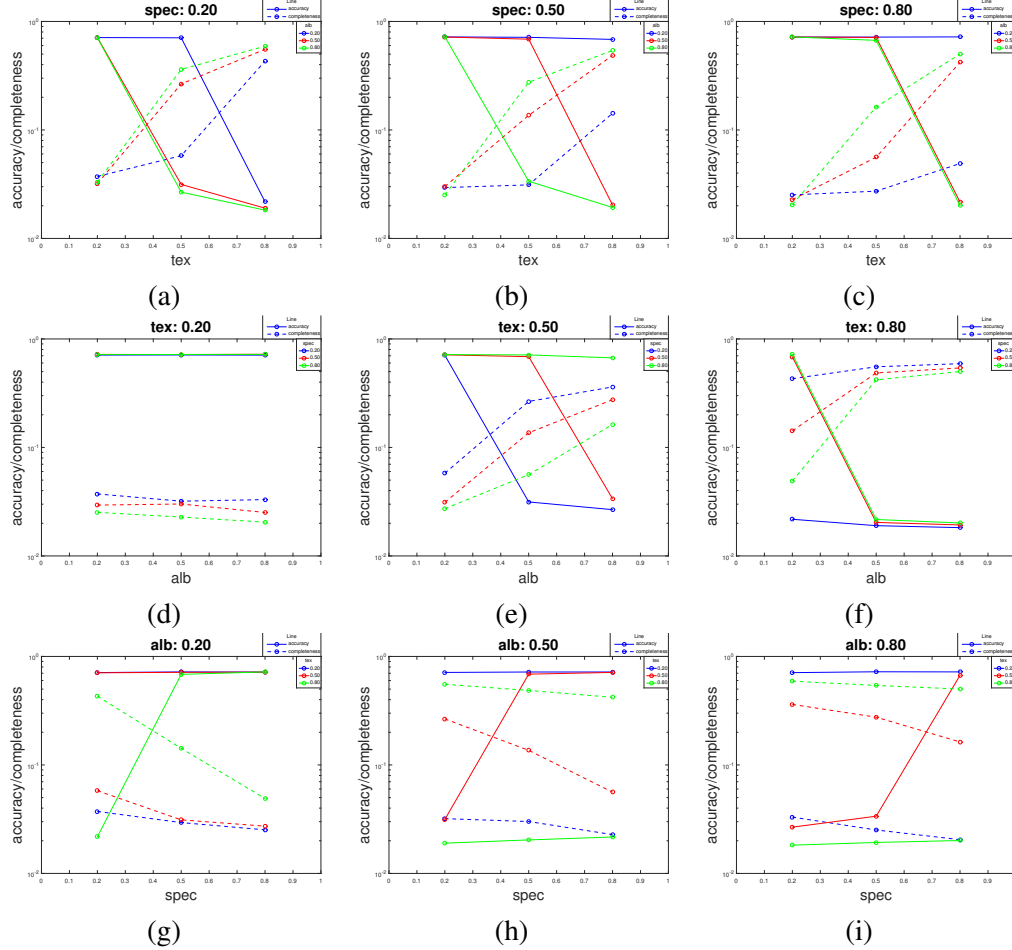


Figure 5.11: Performance of MVS with varied properties.

- (g)-(i):

From all the training results, we could derive the problem conditions that PMVS could reliably work on and get satisfactory results. Those conditions are in Table 5.7.

5.6.2 Example-based PS (EPS)

The performance of example-based PS under difference combinations of properties is shown in Figure 5.12. The conditions that example-based PS works well is listed

| Metric | Texture | Albedo | Specular | Roughness |
|-------------------------|---------|--------|----------|-----------|
| Accuracy & Completeness | 0.8 | 0.2 | 0.2 | - |
| | 0.8 | 0.2 | 0.5 | - |
| | 0.8 | 0.2 | 0.8 | - |
| | 0.8 | 0.5 | 0.5 | - |
| | 0.8 | 0.8 | 0.5 | - |
| | 0.8 | 0.5 | 0.8 | - |
| | 0.8 | 0.8 | 0.8 | - |

Table 5.7: The conditions under which PMVS works well in terms of the two metrics *accuracy* and *completeness*.

in Table 5.8.

We make the following observations from the training results

- (a)-(c): albedo has a positive effect on the reconstruction. Roughness has a more complicated effect on reconstruction, i.e., as roughness would blur the specular area, it might actually make the results worse, see Figure 5.7.
- (d)-(f): the effect of specular is that it will create ‘spikes’, as shown in Figure 5.6, and albedo can effectively alleviate that.
- (g)-(i): as stated previously, roughness has a more complicated effect on reconstruction, i.e., as roughness would blur the specular area, it might actually make the results worse.

From all the training results, we could derive the problem conditions that EPS could reliably work on and get satisfactory results. Those conditions are in Table ??.

5.6.3 Gray-code SL (GSL)

The performance of Gray code SL under different combinations of properties is shown in Figure 5.13. The conditions that PMVS works well is listed in Table ??.

From all the training results, we could derive the problem conditions that GSL could reliably work on and get satisfactory results. Those conditions are in Table 5.9.

| Metric | Texture | Albedo | Specular | Roughness |
|------------------|---------|--------|----------|-----------|
| Angle difference | - | 0.8 | 0.2 | 0.2 |
| | - | 0.8 | 0.5 | 0.2 |
| | - | 0.8 | 0.8 | 0.2 |
| | - | 0.2 | 0.2 | 0.8 |
| | - | 0.2 | 0.5 | 0.8 |
| | - | 0.2 | 0.8 | 0.8 |
| | - | 0.5 | 0.2 | 0.8 |
| | - | 0.5 | 0.5 | 0.8 |
| | - | 0.5 | 0.8 | 0.8 |
| | - | 0.8 | 0.2 | 0.8 |
| | - | 0.8 | 0.5 | 0.8 |
| | - | 0.8 | 0.8 | 0.8 |

Table 5.8: The conditions under which example-based PS works well in terms of the two metric *angular difference*.

| Metric | Texture | Albedo | Specular | Roughness |
|--------------|---------|--------|----------|-----------|
| Accuracy | - | - | - | - |
| Completeness | - | 0.2 | 0.5 | 0.8 |
| | - | 0.2 | 0.8 | 0.8 |
| | - | 0.5 | 0.2 | 0.8 |
| | - | 0.5 | 0.5 | 0.8 |
| | - | 0.5 | 0.8 | 0.8 |
| | - | 0.8 | 0.2 | 0.5 |
| | - | 0.8 | 0.5 | 0.5 |
| | - | 0.8 | 0.8 | 0.5 |
| | - | 0.8 | 0.2 | 0.8 |
| | - | 0.8 | 0.5 | 0.8 |
| | - | 0.8 | 0.8 | 0.8 |

Table 5.9: The conditions under which Gray code SL works well in terms of the two metrics *accuracy* and *completeness*.

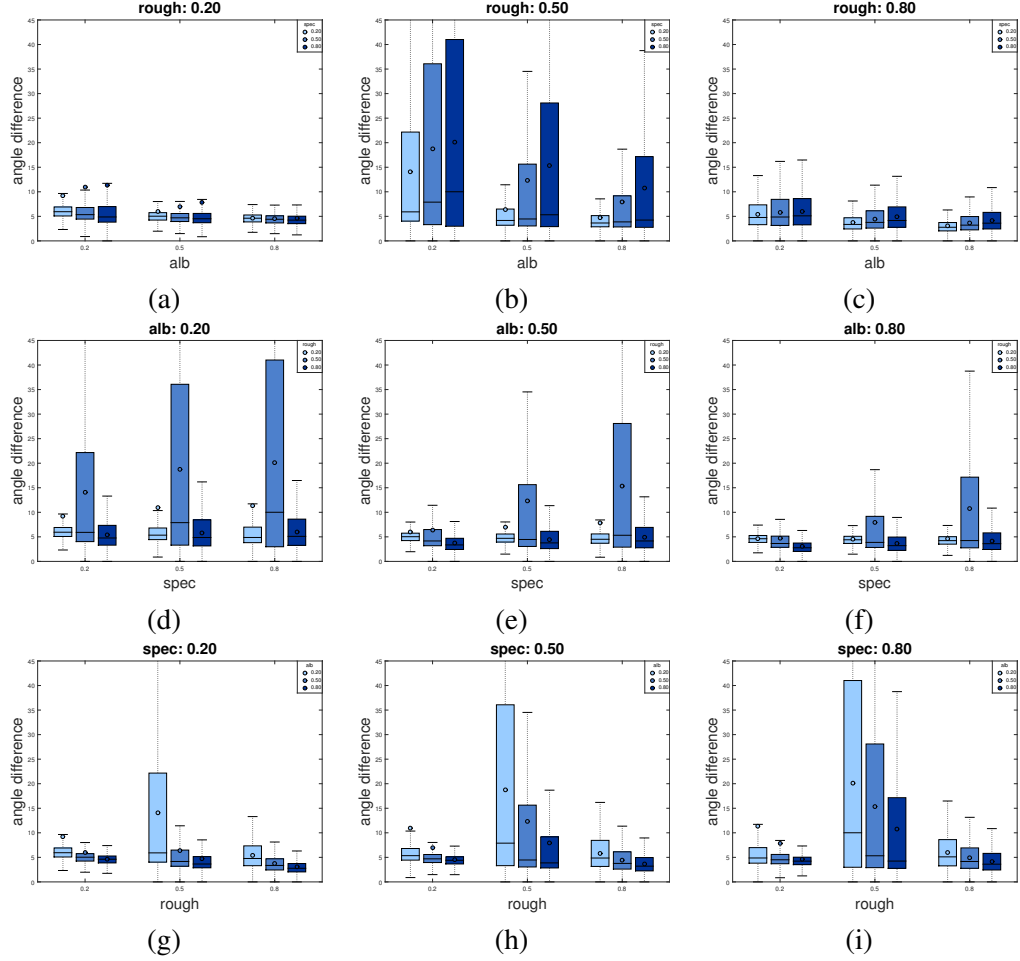


Figure 5.12: Performance of PS with varied properties.

5.7 Mapping

From the training results, we can derive the problem conditions under which each algorithm works well. The next step is to find the best possible algorithm based on the problem description. This could result in multiple algorithms selected, or none selected for some cases. Nonetheless, we need to establish the rule of determining which algorithm gives the best result under the specified conditions.

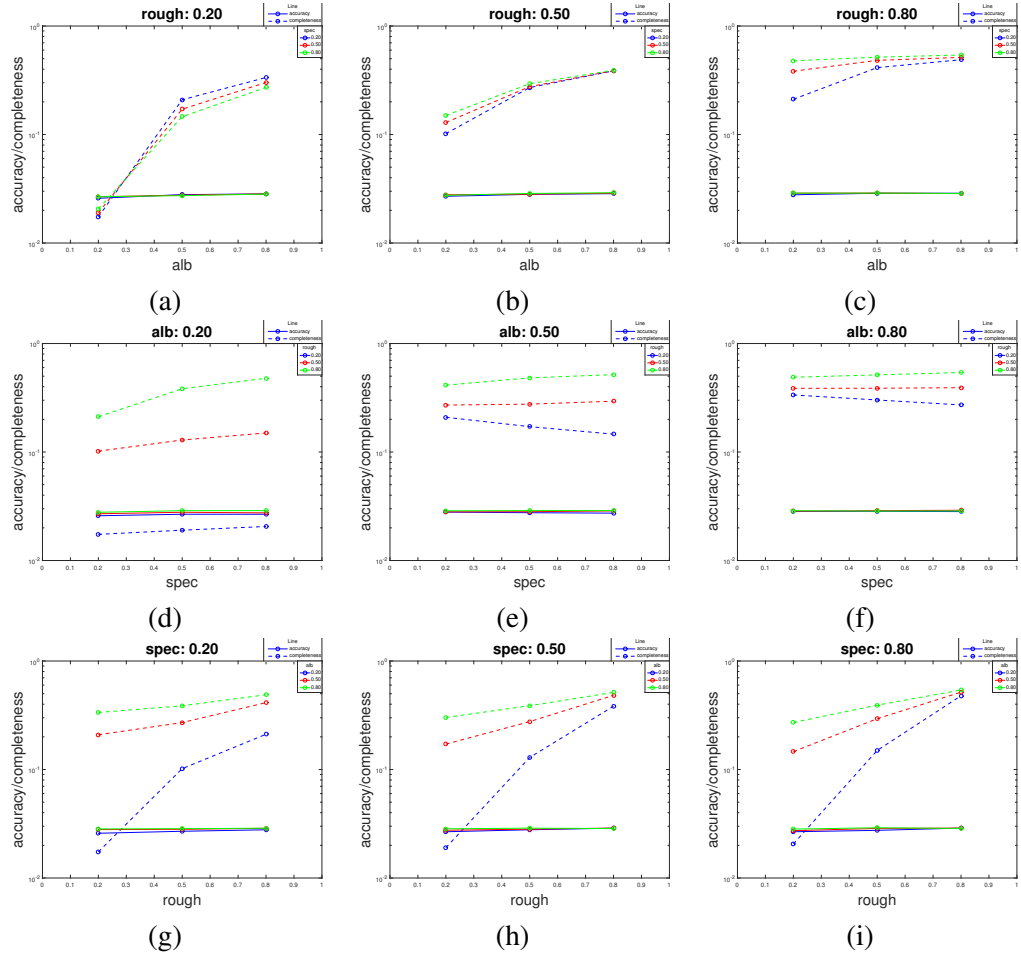


Figure 5.13: Performance of SL with varied properties.

Chapter 6

An Interpretation of 3D Reconstruction

In Chapter 5, we have established a mapping from a well defined problem space to a suite of algorithms through evaluating the performance under synthetic situations. However, the claim that this mapping is useful in terms of helping users find the best possible algorithm given problem conditions, or easing the use of complicated vision algorithm, is still unclear. Thus a thorough evaluation is needed to answer those questions.

However, such an evaluation faces several challenges: 1). the derived mapping doesn't pose strict constraints on the type of material and geometry, thus the evaluation should target a vast amount of objects to reach a solid conclusion, which is obvious not a practical approach; 2). the sense of ease of use is a fairly objective measure, the typical method is conduct user experiments. However, user studies is also limited that it only tests the performance for a small set of algorithms and a small set of conditions. Without covering a large range of possibilities, the results would be biased or even wrong. For instance, ??. Thus a new approach is needed to measure the complexity of the traditional the newly proposed way of reconstructing an object, which should be independent to problem space and selected algorithms.

Although only three algorithms selected, all of which are the top performers in the corresponding field, thus are sufficient to demonstrate the framework's ability

to translate the descriptive model into a reconstruction. Furthermore, the integration of a new algorithm requires the same process presented in Chapter 5, allowing researchers to contribute novel algorithms to the framework.

6.1 Evaluation Methodology

To prove that the proposed mapping from a condition to an algorithm is a valid one, we need to construct a rigorous evaluation method. In this section, we deal with the steps that are involved to validate the mapping, and the underlying theory to support it.

6.1.1 Objective

This evaluation intends to test the effectiveness and robustness of the derived mapping in Chapter 5.

6.1.2 Key Evaluation Questions and Steps

The most important questions we should always ask when coming up with something new is: 1). *does the proposed framework work?*; 2). *is it an improvement to previous method?*. To put it more formally, the two key questions we need to address or evaluate for the derived mapping is

1. Effectiveness: Does the mapping return the best-possible result?

Given a correct description of the object, the algorithm chosen by the mapping should give the best reconstruction result. We use both synthetic and real-world data to test if this is indeed true. For the synthetic data, the quantitative result is possible due to the ground truth. However, the quantitative results are not available for real-world data since we don't have the groundtruth. We use the same quantitative metrics used in Chapter 5. Therefore, visual analysis is utilized for real-world objects. We use the quantitative measure from Chapter 5.

The evaluation steps are:

- Data collection: the synthetic data is generated by the Blender using the same setups in Chapter 5. The real-world data are captured using different setups:

for MVS, a Nikon D700 camera with [focal] lens are used; for photometric images, a Nikon D700 camera with [focal] lens, and a handheld lamp are used; for structured light images, a Nikon 700 camera and a [??] projector are used.

- Synthetic data: since the ground truth is available, we need to compare both the quantitative results and qualitative results to the result from the mapping to see if they are consistent.
- Real-world data: since the ground truth is not available, we only visually analyse the quality of the reconstruction and see if it's consistent with the mapping.

6.2 Parameter Setting

We provide results from three different descriptions where each activates a different algorithm and provides a demonstrative result. To address if the derived mapping works, The first step of the process is to estimate the amount of property in the object. We use a try-and-fit approach, where the user change the value of each property and see if the rendered result looks alike the real object. A similar approach can be found in the [11] where the author also used a synthetic dataset to find the contributing factors of PS.

6.3 Effectiveness of Mapping

We first evaluate that the derived mapping does what it meant to do: return the best algorithm given a correct description of the object. The idea is that given the description of an arbitrary object, we use all three techniques for reconstruction, and see if the algorithm that has the best quantitative or qualitative result is consistent to the algorithm chosen by the mapping.

6.3.1 Synthetic Datasets

We use one object shown in Figure 6.2, and four property settings in Table 6.1 to test the validity of the abstraction. Those four settings represents four classes

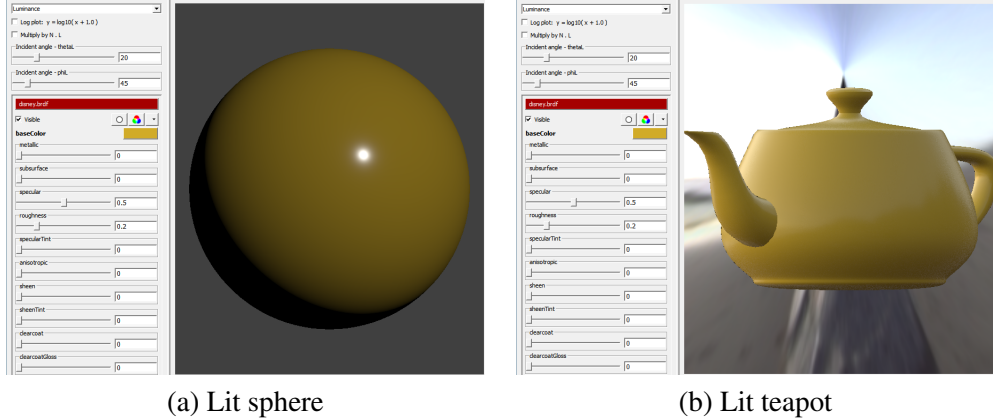


Figure 6.1: The UI of determining the albedo, specular, and roughness of the surface. The albedo is set as around 0.8, which is determined by the value channel of HSV colour. The specular and roughness is set as 0.5, 0.2, respectively. (a) demonstrates the effect of the property setting on a sphere while (b) on a teapot.

of objects discussed in Chapter 4. The best suited algorithm as suggested by the mapping derived from Chapter 5 is included.

| Property | Texture | Albedo | Specular | Roughness | Best-suited techniques |
|----------|---------|--------|----------|-----------|------------------------|
| (a) | 0.2 | 0.8 | 0.2 | 0.8 | PS, SL |
| (b) | 0.2 | 0.8 | 0.5 | 0.2 | PS, SL |
| (c) | 0.8 | 0.8 | 0.2 | 0.8 | MVS, PS, SL |
| (d) | 0.8 | 0.8 | 0.5 | 0.2 | MVS, PS, SL |

Table 6.1: Property lists of the test objects.

Now we show both the quantitative results and qualitative results of the test objects, and see if the results is consistent with the techniques selected by our abstraction. The result is shown in Figure 6.3.

Results

(a), (b) In Figure 6.3 (a), the mapping predicts that EPS and GSL can give satisfactory results, which is consistent to the quantitative result shown in column 2 and the qualitative resulted labeled in red rectangle. The completeness of the PMVS is

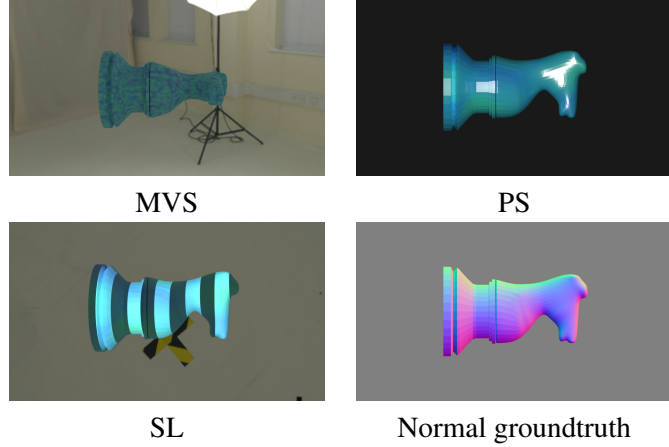


Figure 6.2: The synthetic datasets and groundtruth for the evaluation

low due to the lack of texture.

(c), (d) In Figure 6.3 (a), the mapping predicts that all three methods can give satisfactory results, which is consistent to the quantitative result shown in column 2 and the qualitative resulted labeled in red rectangle.

6.3.2 Real-world Datasets

We used a similar setup to the synthetic settings and captured a real world dataset for nine objects. The property of these objects are listed in Table ???. Since we don't have the ground truth, we resort to visual analysis to see if the algorithm gives the best reconstruction is consistent to the algorithm suggested by the mapping. We choose four representative objects as representatives of the six classes of objects, they are

We use the aforementioned methods to retrieve the parameters of each property, the decomposition of material for each object is presented in Figure A.1.

From the the decomposition of the material, we can have the property matrix shown in Table A.2.

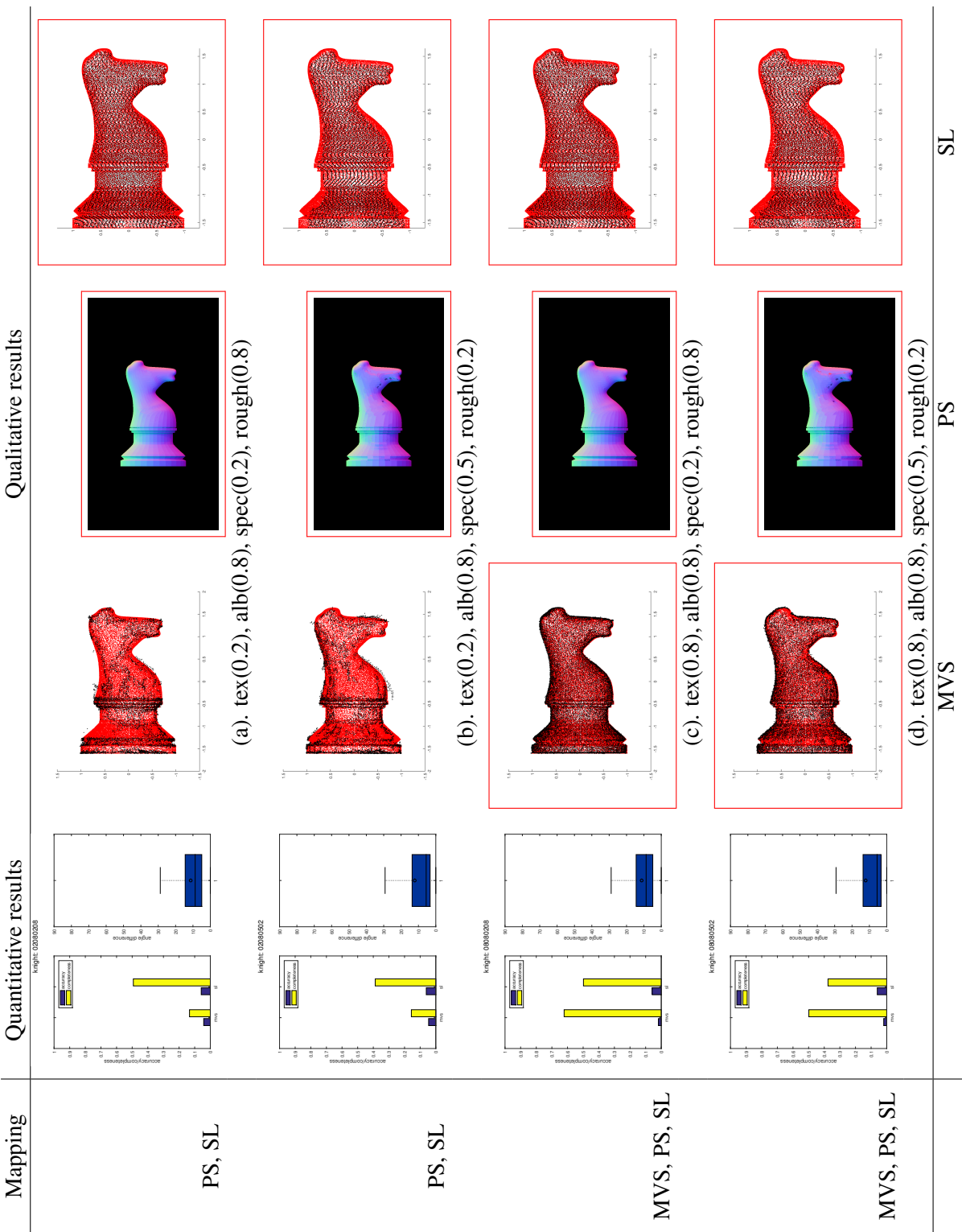


Figure 6.3: The first column shows the best algorithm chosen by the mapping. The quantitative and qualitative performance of each technique on the synthetic dataset. The red dots are from the ground truth while the black ones are the reconstruction.

| class # | 1 | 2 | 3&4 | 5&6 |
|-------------|----------------------------------|------------------------------------|------------------------------------|--------------------------------------|
| description | textureless diffuse bright | textureless mixed d/s bright | textured diffuse dark/bright | textured mixed d/s dark/bright |
| object | | | | |

Figure 6.4: The representatives of the six classes of objects used for evaluation.

| Property | Texture | Albedo | Specular | Roughness | Best-suited Algo. |
|----------|---------|----------|----------|-----------|-------------------|
| status | 0.2 | 0.8 | 0.2 | 0.5 | PS, SL |
| cup | 0.2 | 0.8 | 0.2 | 0.2 | PS, SL |
| pot | 0.5 | 0.2, 0.5 | 0.2 | 0.2 | MVS, SL |
| vase | 0.8 | 0.8, 0.2 | 0.2 | 0.2 | None |

Table 6.2: Property list for the real-world objects

6.4 Robustness of Mapping

Aside from testing whether the description would be correctly mapped to the best algorithm, we should also test given incorrect description, would the mapping return the algorithm that gives less satisfactory results.

As presented in the evaluation steps, we need to give both correct and incorrect description to an object and see if the mapping would give the same mapped algorithm or actually would return difference ones.

6.5 Summary

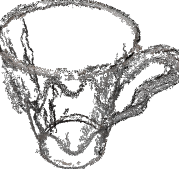
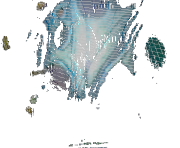
| Object | Mapping | Qualitative results | | |
|--------|---------|---|--|---|
| | | PMVS | EPS | GSL |
| vase | PS, SL |  |  |  |
| cup | PS, SL |  |  |  |
| pot | MVS |  |  |  |
| vase | MVS |  |  |  |

Figure 6.5: The evaluation of the effectiveness of the mapping using real-world object. The well reconstructed object is label by red rectangle.

Bibliography

- [1] Autodesk. URL <http://en.wikipedia.org/wiki/Autodesk>. → pages 1
- [2] Lidar. URL <http://en.wikipedia.org/wiki/Lidar>. → pages 1
- [3] Kinect. URL <http://en.wikipedia.org/wiki/Kinect>. → pages 1
- [4] Vxl c++ libraries for computer vision research and implementation.
<http://vxl.sourceforge.net>. → pages 8
- [5] N. Alldrin, T. Zickler, and D. Kriegman. Photometric stereo with non-parametric and spatially-varying reflectance. In *Computer Vision and Pattern Recognition, 2008. CVPR 2008. IEEE Conference on*, pages 1–8. IEEE, 2008. → pages 24, 30, 33
- [6] N. G. Alldrin and D. J. Kriegman. Toward reconstructing surfaces with arbitrary isotropic reflectance: A stratified photometric stereo approach. In *2007 IEEE 11th International Conference on Computer Vision*, pages 1–8. IEEE, 2007. → pages 16, 31
- [7] N. G. Alldrin, S. P. Mallick, and D. J. Kriegman. Resolving the generalized bas-relief ambiguity by entropy minimization. In *Computer Vision and Pattern Recognition, 2007. CVPR'07. IEEE Conference on*, pages 1–7. IEEE, 2007. → pages 24
- [8] C. Barnes, E. Shechtman, A. Finkelstein, and D. B. Goldman. PatchMatch: A randomized correspondence algorithm for structural image editing. *ACM Transactions on Graphics (Proc. SIGGRAPH)*, 28(3), Aug. 2009. → pages 11
- [9] S. Barsky and M. Petrou. The 4-source photometric stereo technique for three-dimensional surfaces in the presence of highlights and shadows. *IEEE Transactions on Pattern Analysis and Machine Intelligence*, 25(10):1239–1252, 2003. → pages 16, 24, 30, 33

- [10] P. N. Belhumeur, D. J. Kriegman, and A. L. Yuille. The bas-relief ambiguity. *International journal of computer vision*, 35(1):33–44, 1999. → pages 24, 29, 33
- [11] S. Berkiten and S. Rusinkiewicz. An RGBN benchmark. Technical report, Technical Report TR-977-16, Princeton University, Feb. 2016. → pages 48, 70
- [12] F. Bernardini, H. Rushmeier, I. M. Martin, J. Mittleman, and G. Taubin. Building a digital model of michelangelo’s florentine pieta. *IEEE Computer Graphics and Applications*, 22(1):59–67, 2002. → pages 1
- [13] F. Blais. Review of 20 years of range sensor development. *Journal of Electronic Imaging*, 13(1), 2004. → pages 10
- [14] R. C. Bolles and P. Horaud. 3dpo: A three-dimensional part orientation system. *The International Journal of Robotics Research*, 5(3):3–26, 1986. → pages 38
- [15] G. Bradski and A. Kaehler. *Learning OpenCV: Computer vision with the OpenCV library.* ” O’Reilly Media, Inc.”, 2008. → pages 8
- [16] E. N. Coleman and R. Jain. Obtaining 3-dimensional shape of textured and specular surfaces using four-source photometry. *Computer graphics and image processing*, 18(4):309–328, 1982. → pages 16, 24, 30, 33
- [17] C. H. Esteban and F. Schmitt. Silhouette and stereo fusion for 3d object modeling. *Computer Vision and Image Understanding*, 96(3):367–392, 2004. → pages 10, 24, 28
- [18] O. Faugeras and R. Keriven. *Variational principles, surface evolution, pde’s, level set methods and the stereo problem*. IEEE, 2002. → pages 1, 10, 24, 28
- [19] Y. Furukawa. *High-fidelity image-based modeling*. University of Illinois at Urbana-Champaign, 2008. → pages 28
- [20] Y. Furukawa and J. Ponce. Accurate, dense, and robust multiview stereopsis. *IEEE transactions on pattern analysis and machine intelligence*, 32(8):1362–1376, 2010. → pages 1, 11, 24, 33, 49
- [21] S. Galliani, K. Lasinger, and K. Schindler. Massively parallel multiview stereopsis by surface normal diffusion. In *Proceedings of the IEEE International Conference on Computer Vision*, pages 873–881, 2015. → pages 11

- [22] J. Geng. Structured-light 3d surface imaging: a tutorial. *Advances in Optics and Photonics*, 3(2):128–160, 2011. → pages 22
- [23] M. Goesele, B. Curless, and S. M. Seitz. Multi-view stereo revisited. In *2006 IEEE Computer Society Conference on Computer Vision and Pattern Recognition (CVPR'06)*, volume 2, pages 2402–2409. IEEE, 2006. → pages 1, 11, 24, 28, 33
- [24] D. B. Goldman, B. Curless, A. Hertzmann, and S. M. Seitz. Shape and spatially-varying brdfs from photometric stereo. *IEEE Transactions on Pattern Analysis and Machine Intelligence*, 32(6):1060–1071, 2010. → pages 16, 24, 30, 33
- [25] H. Hayakawa. Photometric stereo under a light source with arbitrary motion. *JOSA A*, 11(11):3079–3089, 1994. → pages 15, 24, 29, 33
- [26] A. Hertzmann and S. M. Seitz. Example-based photometric stereo: Shape reconstruction with general, varying brdfs. *IEEE Transactions on Pattern Analysis and Machine Intelligence*, 27(8):1254–1264, 2005. → pages 16, 24, 27, 29, 33, 49
- [27] V. H. Hiep, R. Keriven, P. Labatut, and J.-P. Pons. Towards high-resolution large-scale multi-view stereo. In *Computer Vision and Pattern Recognition, 2009. CVPR 2009. IEEE Conference on*, pages 1430–1437. IEEE, 2009. → pages 10
- [28] B. K. Horn. Shape from shading: A method for obtaining the shape of a smooth opaque object from one view. 1970. → pages 13, 24, 33
- [29] I. Ihrke, K. N. Kutulakos, H. Lensch, M. Magnor, and W. Heidrich. Transparent and specular object reconstruction. In *Computer Graphics Forum*, volume 29, pages 2400–2426. Wiley Online Library, 2010. → pages 23
- [30] S. Inokuchi. Range-imaging system for 3d object recognition. In *Proc. of 7th International Conference on Pattern Recognition, 1984*, 1984. → pages 24
- [31] P. D. Kovesi. MATLAB and Octave functions for computer vision and image processing. Available from: <<http://www.peterkovesi.com/matlabfns/>>. → pages 8
- [32] K. N. Kutulakos and S. M. Seitz. A theory of shape by space carving. *International Journal of Computer Vision*, 38(3):199–218, 2000. → pages 1, 10

- [33] M. Levoy, K. Pulli, B. Curless, S. Rusinkiewicz, D. Koller, L. Pereira, M. Ginzton, S. Anderson, J. Davis, J. Ginsberg, et al. The digital michelangelo project: 3d scanning of large statues. In *Proceedings of the 27th annual conference on Computer graphics and interactive techniques*, pages 131–144. ACM Press/Addison-Wesley Publishing Co., 2000. → pages 1
- [34] M. Lhuillier and L. Quan. Match propagation for image-based modeling and rendering. *IEEE Transactions on Pattern Analysis and Machine Intelligence*, 24(8):1140–1146, 2002. → pages 11
- [35] M. Lhuillier and L. Quan. A quasi-dense approach to surface reconstruction from uncalibrated images. *IEEE transactions on pattern analysis and machine intelligence*, 27(3):418–433, 2005. → pages 11
- [36] J. J. Little. *Recovering shape and determining attitude from extended gaussian images*. PhD thesis, 1985. → pages 34
- [37] S. P. Mallick, T. E. Zickler, D. J. Kriegman, and P. N. Belhumeur. Beyond lambert: Reconstructing specular surfaces using color. In *2005 IEEE Computer Society Conference on Computer Vision and Pattern Recognition (CVPR'05)*, volume 2, pages 619–626. Ieee, 2005. → pages 16, 24, 30, 33
- [38] G. Mariottini and D. Prattichizzo. Egt: a toolbox for multiple view geometry and visual servoing. *IEEE Robotics and Automation Magazine*, 3(12), December 2005. → pages 8
- [39] D. Marr. Vision: A computational investigation into the human representation and processing of visual information. 1982. → pages 10
- [40] W. Matusik, C. Buehler, L. McMillan, and S. J. Gortler. An efficient visual hull computation algorithm. *Tech. Rep., MIT LCS Technical Memo 623, MIT Laboratory for Computer Science*, 2002. → pages 24, 32, 33
- [41] S. K. Nayar, K. Ikeuchi, and T. Kanade. Surface reflection: physical and geometrical perspectives. Technical report, DTIC Document, 1989. → pages 43
- [42] G. P. Otto and T. K. Chau. region-growingalgorithm for matching of terrain images. *Image and vision computing*, 7(2):83–94, 1989. → pages 10
- [43] T. Poggio, V. Torre, and C. Koch. Computational vision and regularization theory. *Nature*, 317(6035):314–319, 1985. → pages 9

- [44] C. Rocchini, P. Cignoni, F. Ganovelli, C. Montani, P. Pingi, and R. Scopigno. Marching intersections: an efficient resampling algorithm for surface management. In *Shape Modeling and Applications, SMI 2001 International Conference on*, pages 296–305. IEEE, 2001. → pages 18
- [45] S. Roy and I. J. Cox. A maximum-flow formulation of the n-camera stereo correspondence problem. In *Computer Vision, 1998. Sixth International Conference on*, pages 492–499. IEEE, 1998. → pages 10
- [46] J. Salvi, J. Pages, and J. Batlle. Pattern codification strategies in structured light systems. *Pattern recognition*, 37(4):827–849, 2004. → pages 12, 22
- [47] Y. Sato and K. Ikeuchi. Temporal-color space analysis of reflection. *JOSA A*, 11(11):2990–3002, 1994. → pages 16, 24, 30, 33
- [48] K. Schluns. Photometric stereo for non-lambertian surfaces using color information. In *International Conference on Computer Analysis of Images and Patterns*, pages 444–451. Springer, 1993. → pages 16, 24, 30, 33
- [49] S. M. Seitz and C. R. Dyer. Photorealistic scene reconstruction by voxel coloring. In *Computer Vision and Pattern Recognition, 1997. Proceedings., 1997 IEEE Computer Society Conference on*, pages 1067–1073. IEEE, 1997. → pages 10
- [50] S. M. Seitz, B. Curless, J. Diebel, D. Scharstein, and R. Szeliski. A comparison and evaluation of multi-view stereo reconstruction algorithms. In *2006 IEEE Computer Society Conference on Computer Vision and Pattern Recognition (CVPR’06)*, volume 1, pages 519–528. IEEE, 2006. → pages 1, 22, 49
- [51] B. Shi, Z. Wu, Z. Mo, D. Duan, S.-K. Yeung, and P. Tan. A benchmark dataset and evaluation for non-lambertian and uncalibrated photometric stereo. In *Proceedings of the IEEE Conference on Computer Vision and Pattern Recognition*, pages 3707–3716, 2016. → pages 22
- [52] W. M. Silver. *Determining shape and reflectance using multiple images*. PhD thesis, Massachusetts Institute of Technology, 1980. → pages 16, 24, 26, 27, 29, 33
- [53] R. Szeliski. Rapid octree construction from image sequences. *CVGIP: Image understanding*, 58(1):23–32, 1993. → pages 24, 32, 33

- [54] P. Tan, S. P. Mallick, L. Quan, D. J. Kriegman, and T. Zickler. Isotropy, reciprocity and the generalized bas-relief ambiguity. In *2007 IEEE Conference on Computer Vision and Pattern Recognition*, pages 1–8. IEEE, 2007. → pages 31
- [55] M. Tarini, M. Callieri, C. Montani, C. Rocchini, K. Olsson, and T. Persson. Marching intersections: An efficient approach to shape-from-silhouette. In *VMV*, pages 283–290, 2002. → pages 24, 32, 33
- [56] Y. Uh, Y. Matsushita, and H. Byun. Efficient multiview stereo by random-search and propagation. In *3D Vision (3DV), 2014 2nd International Conference on*, volume 1, pages 393–400. IEEE, 2014. → pages 11
- [57] A. Vedaldi and B. Fulkerson. VLFeat: An open and portable library of computer vision algorithms. <http://www.vlfeat.org/>, 2008. → pages 8
- [58] G. Vogiatzis, P. H. Torr, and R. Cipolla. Multi-view stereo via volumetric graph-cuts. In *Computer Vision and Pattern Recognition, 2005. CVPR 2005. IEEE Computer Society Conference on*, volume 2, pages 391–398. IEEE, 2005. → pages 10
- [59] G. Vogiatzis, C. H. Esteban, P. H. Torr, and R. Cipolla. Multiview stereo via volumetric graph-cuts and occlusion robust photo-consistency. *IEEE Transactions on Pattern Analysis and Machine Intelligence*, 29(12):2241–2246, 2007. → pages 10, 11, 24, 28, 33
- [60] R. J. Woodham. Photometric stereo: A reflectance map technique for determining surface orientation from image intensity. In *22nd Annual Technical Symposium*, pages 136–143. International Society for Optics and Photonics, 1979. → pages 13
- [61] R. J. Woodham. Photometric method for determining surface orientation from multiple images. *Optical engineering*, 19(1):191139–191139, 1980. → pages 1, 14, 24, 26, 29, 33
- [62] E. Zheng, E. Dunn, V. Jojic, and J.-M. Frahm. Patchmatch based joint view selection and depthmap estimation. In *Proceedings of the IEEE Conference on Computer Vision and Pattern Recognition*, pages 1510–1517, 2014. → pages 11
- [63] T. E. Zickler, P. N. Belhumeur, and D. J. Kriegman. Helmholtz stereopsis: Exploiting reciprocity for surface reconstruction. *International Journal of Computer Vision*, 49(2-3):215–227, 2002. → pages 16, 24, 31, 33

Appendix A

Supporting Materials

This would be any supporting material not central to the dissertation. For example:

- radiometry
- technical details of MVS, PS, SL, SfS, etc

A.1 Material of real-world objects

A.2 Parameters of real-world objects

A.3 Results of real-world objects

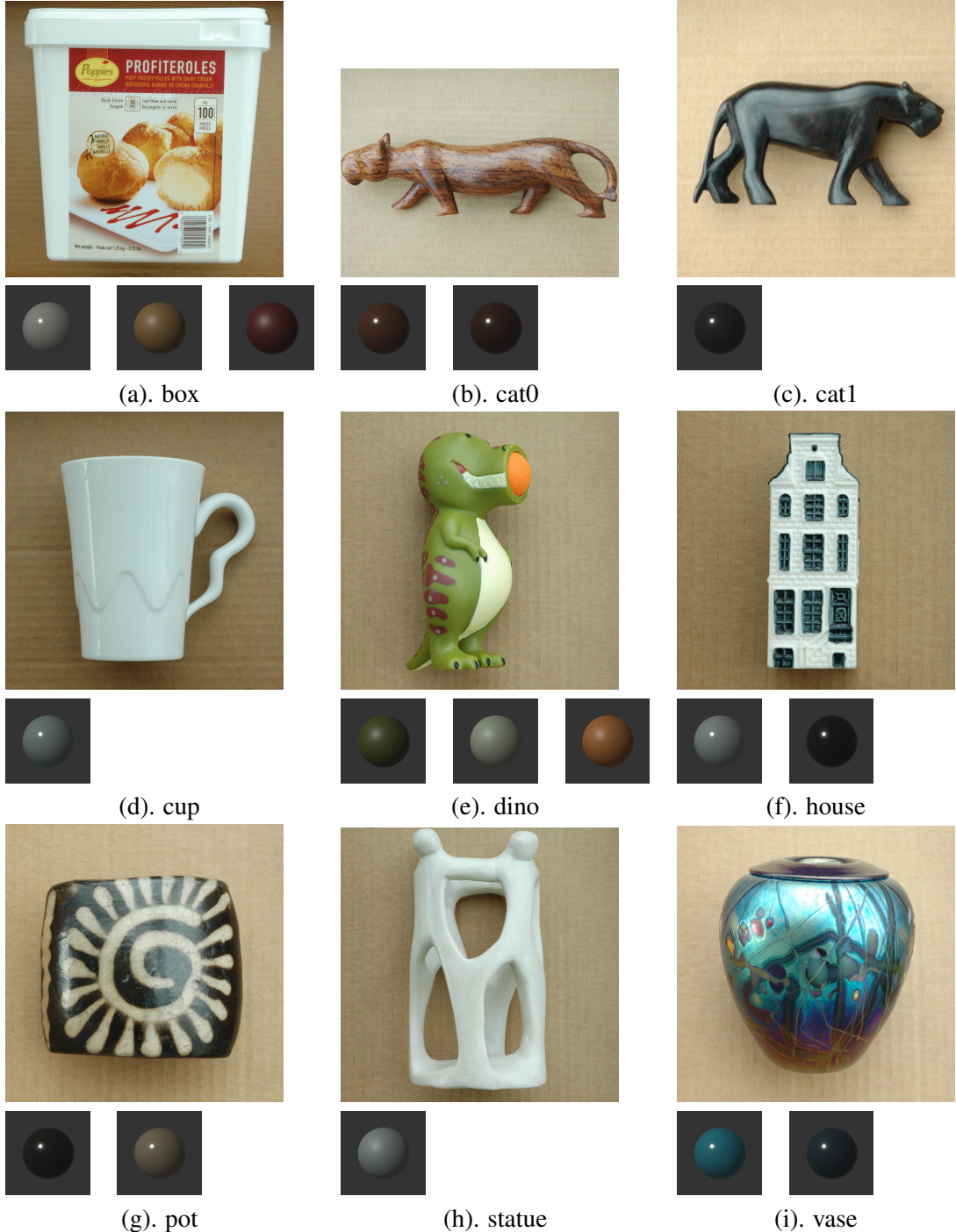


Table A.1: Material of Real-world objects.

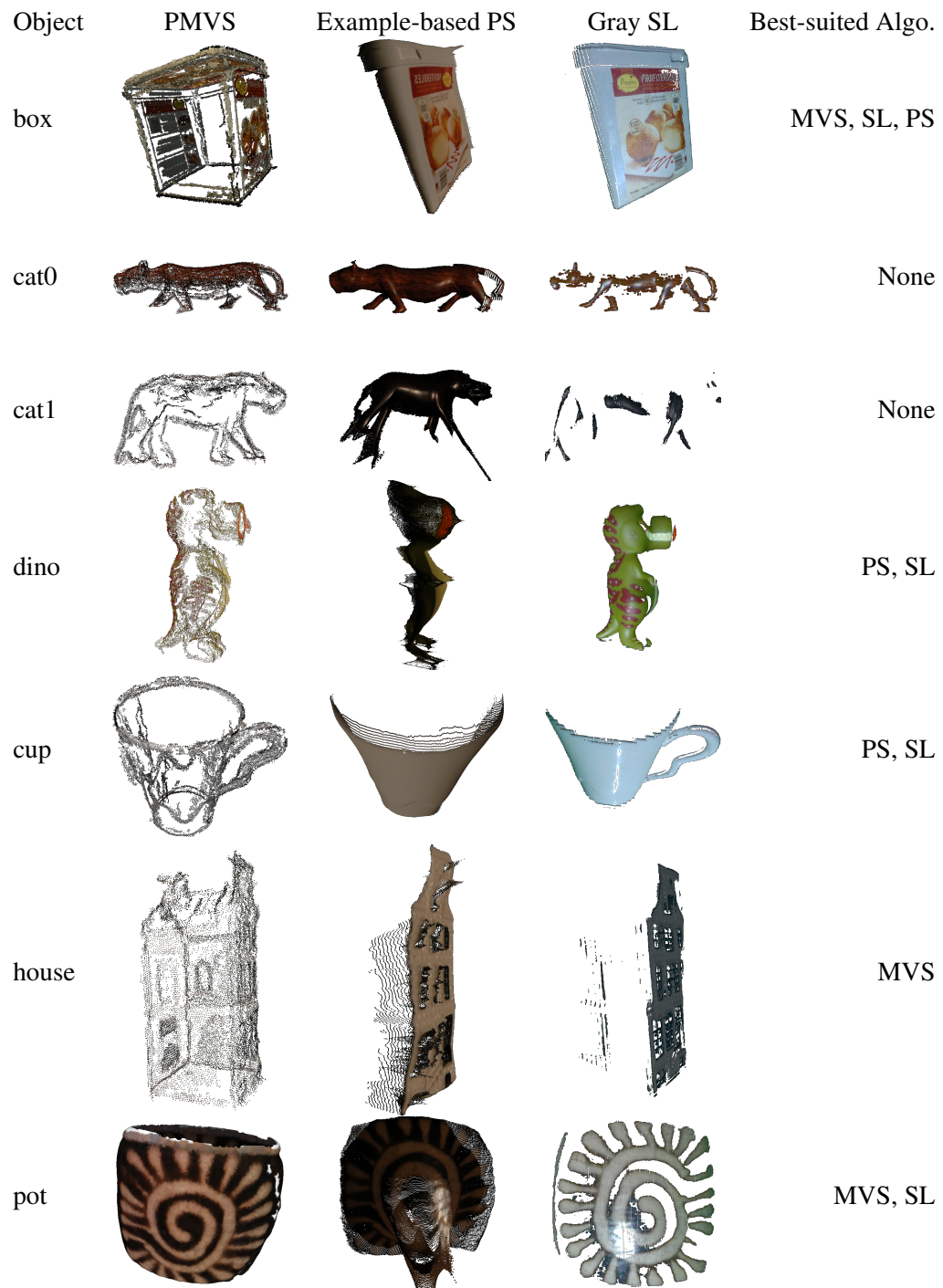


Figure A.1: Reconstruction results of MVS, PS, SL

| Property | Texture | Albedo | Specular | Roughness | Best-suited Algo. |
|-----------------|---------|---------------|----------|-----------|-------------------|
| box | 0.2 | 0.8 | 0.2 | 0.2 | MVS, SL, PS |
| | 0.5 | 0.2 | 0.2 | 0.5 | |
| | 0.8 | 0.8 | 0.2 | 0.5 | |
| cat0 | 0.5 | 0.5, 0.2 | 0.2 | 0.2 | None |
| cat1 | 0.2 | 0.2 | 0.2 | 0.2 | None |
| cup | 0.2 | 0.8 | 0.2 | 0.2 | PS, SL |
| dino | 0.2 | 0.5, 0.8, 0.8 | 0.2 | 0.5 | SL |
| house | 0.8 | 0.8, 0.2 | 0.2 | 0.2 | MVS |
| pot | 0.5 | 0.2, 0.5 | 0.2 | 0.2 | MVS, SL |
| status | 0.2 | 0.8 | 0.2 | 0.5 | PS, SL |
| vase | 0.8 | 0.8, 0.2 | 0.2 | 0.2 | None |

Table A.2: Property list for the real-world objects

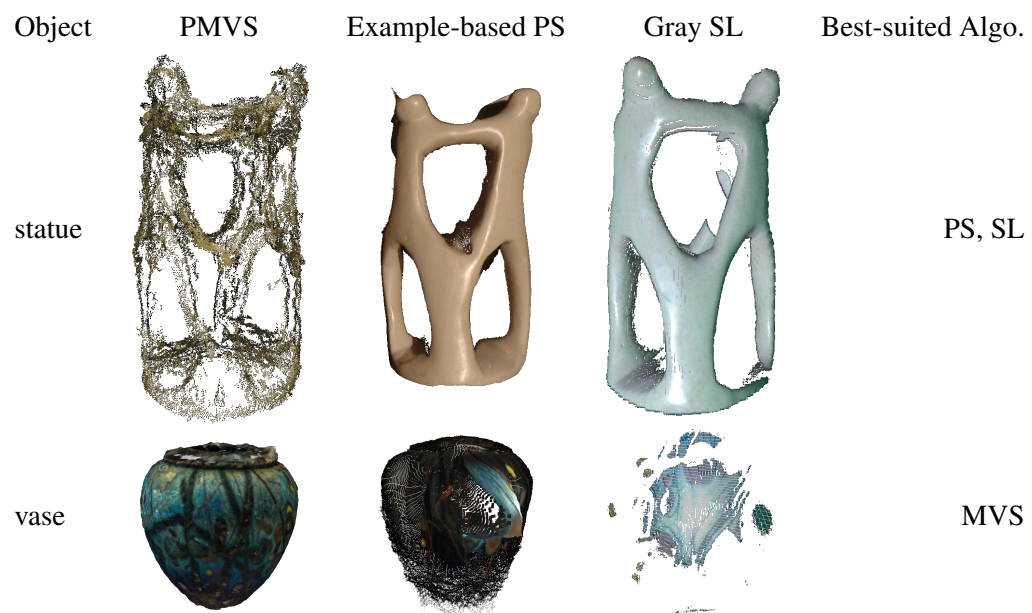


Figure A.2: Reconstruction results of MVS, PS, SL (cont'd)